Received: 1 May 2024 | Revised: 25 October 2024 | Accepted: 25 November 2024

IET Generation, Transmission & Distribution

DOI: 10.1049/gtd2.13343

The Institution of Engineering and Technology WILEY

ORIGINAL RESEARCH

Dynamic sensitivity-based clustering of distributed energy resources using LoRaWAN technology for voltage regulation in distribution networks

Ameen Gargoom[1] | **Mohammed Elmusrati**[2] | **Ahmed Gaouda**[3]

[1]School of Engineering, Deakin University, Geelong, Australia

[2]School of Technology and Innovations, Computing Sciences, University of Vaasa, Vaasa, Finland

[3]Electrical Technology Department, Collage of Electrical and Electronics Technology, Benghazi, Libya

Correspondence
Ameen Gargoom, School of Engineering, Deakin University, Geelong, Australia.
Email: a.gargoom@deakin.edu.au

Abstract

As the penetration level of renewable energies increases, many inverter-based resources (IBRs) managing algorithms are proposed to control the impact of this penetration on the system. Some of these algorithms are based on a local control without visualizing the status of the whole network and others are based on a centralized control approach that results in dynamic settings without considering the mutual sensitivity among different IBRs. Hence, flexible management of IBRs to be simultaneously controlled either locally or remotely and satisfy technical and fair utilization at IBRs and systems levels becomes essential. The proposed flexible management algorithm suggested a dynamic setting that estimates the mutual sensitivity among IBRs at the system level and assures fairness among different owners. This mutual sensitivity link provides a quantifying measure of IBRs injected power on the status of the whole network. Furthermore, this measure defines dynamic clusters' boundaries that are continuously updated by including the most sensitive IBRs and updating their dynamic settings. This update takes place as system configuration, loads, and available sun-power change in order to satisfy the flexible management algorithm without impacting fairness. The algorithm is applied on a sample DN and imposes compliance with system standard limits within a time-frame of the stand-alone LoRaWAN communication platform.

1 | INTRODUCTION

Meeting the Paris Agreement's objective of becoming climate-neutral by 2050 requires building a robust infrastructure capable of monitoring, responding, anticipating, and being inquisitive while managing a vast array of renewable resources. However, the penetration of inverter-based resources (IBRs), mainly household solar panels, in distribution networks (DNs) is already creating significant challenges in both normal and dynamic grid conditions [1]. As IBRs become a predominant source of supply within the DNs, the role of distribution network operators (DNOs) expands, demanding enhanced oversight and control of customer-owned assets to ensure system security, reliability, and equitable distribution of resources.

One of the most critical technical challenges in DNs is voltage limit violation caused by reversed power flow from the IBRs. Studies [2–5] demonstrate that the stochastic nature of IBRs and their mismatch with local loads lead to concerning voltage rises across the DN. To address this and maintain system reliability and security with high penetrations of distributed photovoltaics (DPVs), DNOs are increasingly implementing enhanced power management and curtailment of customer-owned assets, primarily focusing on exported energy, especially during peak PV output. For example, in Australia, historical regulations allowed consumers to install up to 5 kW PV systems per phase with unrestricted export to the grid. However, the rapid rise in PV adoption has prompted distribution companies to progressively tighten export limits, often to 2 kW or 1 kW, and in some cases, completely restrict export [6]. In Victoria alone, three of the largest DNOs (AusNet Services, Powercor, and CitiPower) reduce export levels for 20% to 40% of new connections in response to this issue [6, 7]. This approach, while addressing

voltage issues, does come at a cost to customers. The estimated annual financial losses due to tightening the PV export limits in South Australia alone ranging from $1.2 million to $4.5 million [8].

Alternatively, battery storage, while offering a promising solution for managing power and voltage, over 90% of existing installations lack it, making it an incomplete solution at present. Conversely, the integration of advanced functionalities such as the volt-watt and volt-var in smart inverters [9] has stimulated the emergence of more refined strategies to address the issue of voltage rise [2]. Although reactive power has proven effective for voltage regulation in transmission systems, managing reactive power from inverters in DNs using the volt/var function for voltage regulation remains a challenge. This challenge stems from various factors, including the high inherited R/X ratio in DNs, the relatively small capacity of rooftop inverters which are designed primarily for active power supply, and the typical occurrence of voltage rise during midday when active power generation is at its peak (leaving only limited headroom for reactive power). Additionally, injecting or absorbing reactive power increases reactive current, leading to further losses in the network [10].

Consequently, the use of the volt/watt function has been explored extensively to address the voltage rise in DNs [11]. However, managing the volt/watt function across a large number of inverters has raised valid concerns regarding the fairness of power curtailment among different customers. The radial nature of the typical DNs imposes customer-location profiles which have a direct impact on the voltage rise level. Enforcing simple active power curtailment without implementing fair management of the associated power reduction leads to a form of location-based disadvantages [12]. Thus, the lack of fairness in managing the IBRs represents another financial challenge that can discourage customer engagement for better management of the system [13].

Various approaches have been proposed for integrating fairness into curtailment strategies. These approaches can be broadly divided into power droop-based approaches [14–16], and optimization-based approaches using optimal power flow (OPF) analysis [17–22]. Work in [14] proposed varying droop parameters among PV prosumers for equal curtailment sharing, though this reduced grid energy export. While [15] introduced a droop-based method for fairness, it increased curtailment and computational complexity. An adaptive approach in [16] proposed absorbing reactive power before equitably curtailing active power but required knowledge of other PV systems' parameters and complex signaling patterns to identify voltage violations [23]. Optimization-based strategies have also been explored. While [17] proposed a fair power capping method, it faces limitations with dispersed resources [18] and focuses on periodic rather than instantaneous fairness [24]. Though [19] aims to minimize losses and unfairness, and [20] investigates OPF-based schemes, these approaches lack coordination among DERs. Recent Lagrangian-based methods [21], [22] promote collaborative fairness but depend on optimization solvers [25] and are limited to simplified scenarios [26].

Existing fairness schemes typically focus on equitable distribution of curtailed power, either uniformly or proportionally to generation capacities. However, these approaches often increase overall power curtailment compared to "unfair" methods, with [26] showing that feeder or area-based curtailment distribution can increase total curtailment by 4.71%. Thus, achieving fairness in terms of sharing curtailed power while minimizing total curtailment remains a challenge. This is mainly due to the variations in the sensitivity of the generated power to the voltage rise. Current schemes may require excessive curtailment from customers with minimal voltage impact to compensate for those with substantial impact. An overlooked aspect is linking fairness to each customer's responsibility for voltage rise. This paper proposes a novel fairness scheme addressing these challenges while maximizing PV generation capacity. In this study, fairness is defined as a principle for managing PV curtailment that considers each customer's individual contribution to voltage rise while maximizing overall PV generation capacity. This approach ensures that customers with a higher impact on network voltage bear more responsibility for curtailment, while those with minimal impact are less affected. By aligning curtailment with responsibility, this approach seeks to minimize overall curtailed power, maximize PV generation utilization, and ensure equitable treatment of all participants.

In this context, DNOs face significant challenges in remotely maintaining numerous behind-the-meter single-phase IBRs effectively and fairly due to limited visibility and complex data monitoring. A third-party solution is essential to monitor fairness among IBR owners and develop robust infrastructure zones. The emerging Long-Range Wide Area Network (LoRaWAN) technology enables energy service aggregators (ESA) to coordinate between DNOs and IBR owners, shifting focus towards active IBR management and fair business revenue for customers. This paper proposes LoRaWAN integration as a promising communication option for energy market engagement. Its scalability for managing large numbers of nodes [27–29] makes it attractive for electric DN applications, offering cost-effective visibility at the customer side. This supports DNOs in controlling IBR deployment impacts [30] while allowing fair IBR utilization.

LoRaWAN, a leading Low-Power Wide Area Network technology supported by the LoRa Alliance [31], has been widely adopted for remote intelligent monitoring across various fields [32–39]. In electric power systems, its applications include smart energy metering [32], covering 17 km2 using 19 gateways, demand response programs [33], and synchronized energy measurements [34]. It's also used for smart metering applications [35, 36], complementing 5G networks [37], and supporting large-scale distributed measurement systems [38]. LoRaWAN has been integrated into smart inverter control for remote microgrid applications [39]. The paper proposes a dynamic clustering LoRaWAN-based approach for managing IBRs in distribution networks, focusing on the voltage rise (VR) problem while supporting other applications. The technique links IBR responsibility in VR with fairness to maximize sun-power utilization and minimize overall curtailment. Using voltage-violation time instants, the algorithm employs LoRaWAN to

define dynamic cluster boundaries for IBRs and update their settings. Fairness is based on mutual Voltage-Power sensitivity, with only the most sensitive IBRs being clustered and used for voltage regulation. This approach differs from existing local or centralized control algorithms that may negatively impact adjacent buses or lead to unfair financial benefits due to ignoring mutual sensitivity among IBRs. The main contributions of the paper are summarized as follows:

- A LoRaWAN-based data-driven framework enables flexible local or remote control of IBRs, ensuring fairness in solar power usage and network voltage control. The algorithm addresses fairness in terms of IBR location, power limits, and terminal voltage, with an alternative where only inverter rating and available solar energy serve as constraints.
- A dynamic setting for ensuring dynamic droop control for all IBR-inverters connected in a DN. The proposed dynamic setting identifies which IBRs contribute more to voltage violations, as their power injections lead to a greater increase in bus voltages than others. This allows all IBRs to fairly utilize the maximum available sun-power without violating the voltage limit.
- A new approach is proposed for estimating individual IBR voltage sensitivity to active power changes at other IBR buses. Unlike traditional methods using Jacobian matrices or system impedances, this algorithm develops mutual sensitivity based on IBR droop control. The approach generates voltage sensitivity lines by varying the IBR droop control's low and high break-out values to estimate mutual sensitivity among different IBRs.
- A dynamic clustering approach based on active power mutual sensitivity among IBRs in a DN. Using a developed sensitivity contribution measure, it estimates how voltage-power changes in one IBR impact others. The most sensitive IBRs are clustered to address VR problems while maintaining fairness in sun-power utilization. Clusters dynamically adapt to changes in system configuration, loading conditions, available sun-power, and mutual sensitivities between IBR.

2 | A PROPOSED DYNAMIC DROOP CONTROL

When the IBRs are set to follow a volt-watt and volt-var piecewise linear characteristics (droop) as defined by IEEE 1547–2018 [9], the injected power from the inverter ($P_{j,inv}$) is controlled by the inverter terminal voltage ($E_{j,pu}$). In practice, the power $P_{j,inv}$ is limited by the inverter size, available energy resources, and the selected low and high break-out values ($E_{i,LO}$ and $E_{i,HI}$) that define the inverter's curtailment region. Fixed limits are recommended by the standard for all inverters (IEEE std. 1547). These limits have a significant impact on the amount of curtailed power, the fairness of the curtailment, and the speed of voltage regulation. Changing these limits from fixed to dynamic makes the droop control dynamic and allows for more flexibility in operations. Thus, a dynamic droop is proposed as below.

2.1 | The dynamic droop description and setting

In the proposed dynamic droop control algorithm, while a fixed value is assigned to the high break-out ($E_{i,HI}$), a dynamic (not fixed) low break-out ($E_{i,LO}$) is implemented. This is illustrated in Figure 1a. The possible maximum dynamic low and high values (Min_{DY-LO} and Max_{DY-LO}, respectively) are defined based on the range of the terminal local voltage and the violation limit set by the system operator. In the proposed dynamic droop control, the IBRs continuously update their limits according to the following relations:

$$Min_{DY-LO} \le E_{i,LO} \le Max_{DY-LO}, \tag{1}$$

$$E_{i,LO} = (\beta\%)\, E_i, Min_{DY-LO} \le E_i < Max_{DY-LO}, \tag{2}$$

$$\begin{gathered} E_{i,LO} = Max_{DY-LO} \\ Max_{DY-LO} \le E_i \le violation\ limit' \end{gathered} \tag{3}$$

$$\begin{gathered} E_{i,LO} = Max_{DY-LO}\left(e^{-\gamma[E_i - Max_{DY-LO}]}\right). \\ E_i > violation\ limit \end{gathered} \tag{4}$$

These limits are gradually changed based on the selected decaying factor (γ) taking into consideration both scenarios of entering or leaving the violation limit. The $\beta\%$ factor is selected to make $E_{i,LO}$ heading the IBR voltage by a small percentage. Figure 1b,c shows the proposed dynamic droop control that varies the low break-out ($E_{i,LO}$) and its impact on the terminal voltage and the IBR injected power as compared with applying IEEE std. setting. The results are based on setting Min_{DY-LO} and Max_{DY-LO} to 1.05 and 1.075 pu and a violation limit of 1.080 pu. Note once the inverter enters the dynamic droop mode, it can adjust its low break-out limits based on local voltage measurements without communications, as long as the limit stays within the maximum allowed value.

2.2 | The performance of dynamic-droop against the fixed-droop and the concept of injected power responsibility

2.2.1 | A case when the IBR's injected power is not responsible for the voltage rise

Figure 2a shows the voltage-power interaction response of IBR according to the IEEE std. (a fixed droop control). The IBR's terminal voltage ($E_{i,inv}$) and its generated power ($P_{i,inv}$) are plotted in per unit scale in Figure 2a to illustrate the voltage-power interaction.

The time t_o denotes the instant at which the terminal voltage exceeds the lower limit ($E_{i,inv} > E_{i,LO}$) causing the IBR to enter the droop mode (the shaded grey area in Figure 2a). During this mode, the inverter's power ($P_{i,inv}$) is bounded by the droop line which is defined by the droop low and high break-out values ($E_{i,LO}$ and $E_{i,HI}$) as shown in Figure 2b. Consequently, while

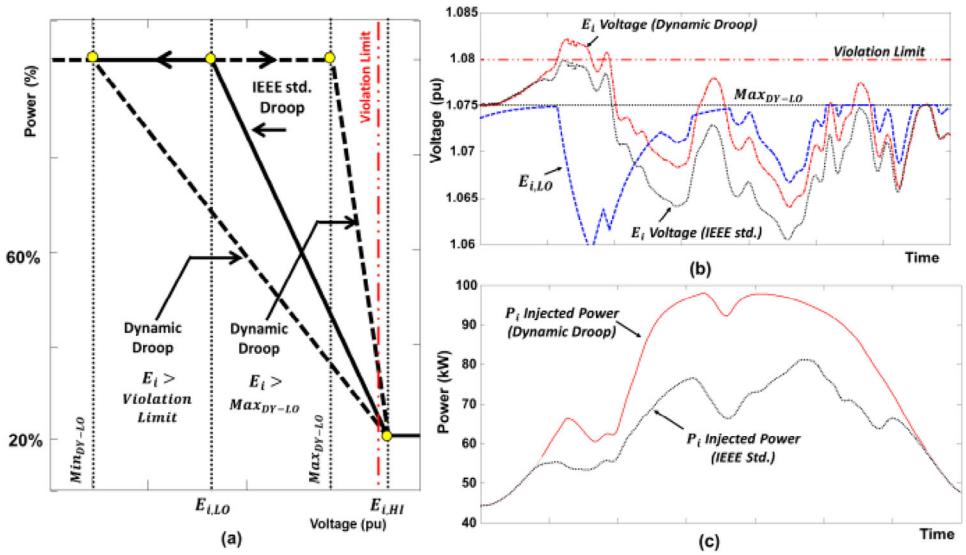

FIGURE 1 (a) The proposed dynamic droop control, (b) the impact of the terminal voltage on the dynamic low limit, and (c) the inverter power.

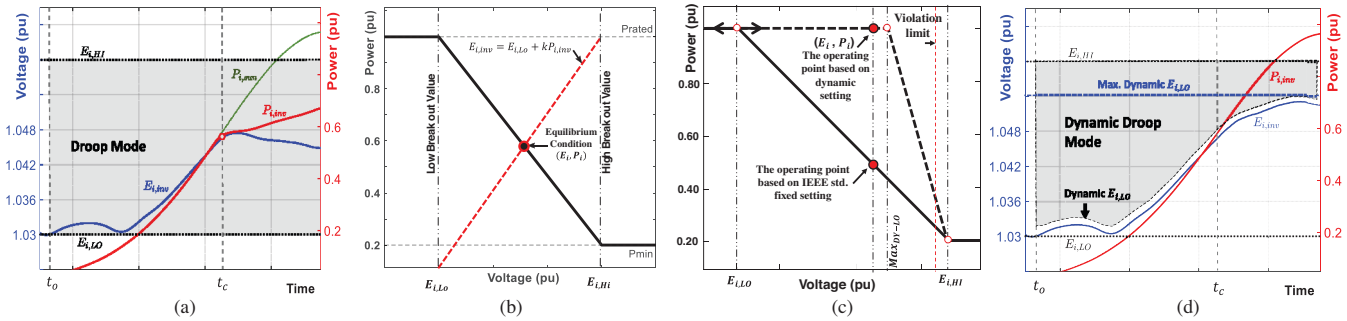

FIGURE 2 (a) Voltage-power interaction of IBR_i using IEEE std fixed settings, (b) the settled point (operating condition) during droop mode, (c) IEEE std. fixed droop and dynamic droop control, and (d) voltage-power interaction of IBR_i using dynamic settings.

$P_{i,inv} \leq$ the droop line, the generated power $P_{i,inv}$ will continue to increase during the droop mode, (following the available $P_{i,sun}$) causing a further rise in the terminal voltage. Thus, $P_{i,inv}$ will not be curtailed unless its value exceeds the sloped droop line. This response is illustrated in Figure 2a where both $P_{i,inv}$ and $E_{i,inv}$ continued to increase after $E_{i,inv} > E_{i,LO}$ and $P_{i,inv}$ was curtailed only after the time-instant (t_c). This delay can be explained based on our definition of the equilibrium principle concept in the droop control as illustrated in Figure 2b. When the inverter enters the droop control mode, the relationship between $P_{i,inv}$ and $E_{i,inv}$ can be expressed as

$$P_{i,inv} = m_{droop}\, E_{i,inv} + C, \tag{5}$$

where m_{droop} represents the slope of the droop line.

The voltage $E_{i,inv}$ is also a function of the power at the bus i and the network configuration. However, for small variations between ($E_{i,LO}$, $E_{i,HI}$), the voltage $E_{i,inv}$ can be approximated as

$$E_{i,inv} = E_{i,LO} + k\, P_{i,inv}, \tag{6}$$

where k is a coefficient related to the loading condition and network condition. The simultaneous solution of (5) and (6) generates the equilibrium point (the operating point) shown in Figure 2b, at which the voltage and power settle at time t_c following some time delay response depends on system condition.

The interaction between the $P_{i,inv}$, $E_{i,inv}$, the loading condition, and the system configuration define the time duration required from t_o to t_c, and thus the location of the operating point (E_i, P_i) on the droop line. It is worth mentioning that if $E_{i,inv}$ is not impacted by any other adjacent inverters or other changes in the load or system conditions, the operating point will remain constant on the droop line. However, in real scenarios, other inverters and system conditions cause the operation point to vary (to slide up and down on the droop line as long the available sun-power is higher than the droop line power $P_{i,sun} \geq P_{i,inv}$). Figure 2c is used to compare the operating points (the red dots) at the time instant t_c in case of a fixed droop control (solid line) and in case of a dynamic droop (dotted line).

It should be noted here, in a system with distributed inverters, monitoring locally the voltage-power interaction in a fixed droop approach does not give any indication of whether the

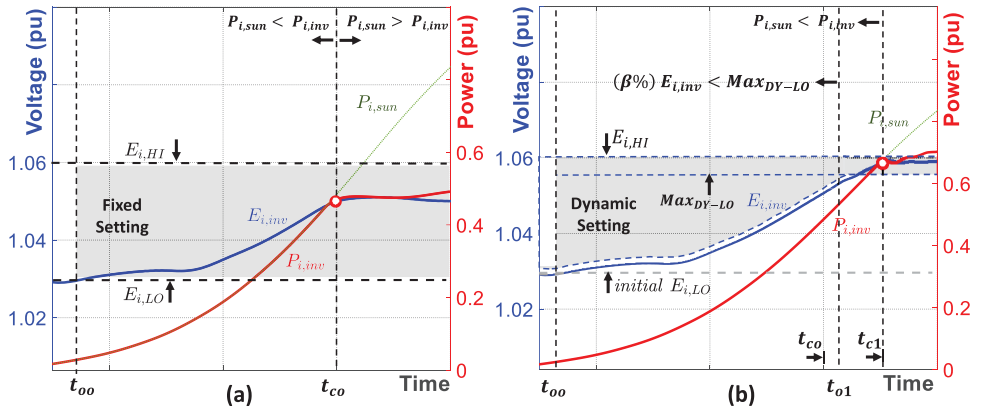

FIGURE 3 A comparison of the fixed and dynamic settings. (a) IEEE std. fixed setting and (b) dynamic setting.

generated power ($P_{i,\text{inv}}$) of the local IBR_i is the main source of (or has a significant impact on) the voltage rise ($E_{i,\text{inv}}$); or the contribution of the injected power from the other IBR_s (distributed in the system) is the main source of this voltage rise. This is because once IBR_i enters the droop mode and its power exceeds the droop line, the droop control automatically forces the IBR_i to operate at a specific point (E_i, P_i) between $E_{i,LO}$ and $E_{i,HI}$ without examining voltage-power interaction and its impact on voltage rise. Furthermore, the operation of the IBR_i during the droop mode and after the time t_c has a direct impact on the fairness condition among different IBR-owners. The droop control restricts IBR_i from utilizing the available sun power without any indicator that increasing $P_{i,\text{inv}}$ is a source of voltage rise (locally or globally) beyond a violation standard limit in the DN.

For the purpose of comparison, the previous case of IBR_i is considered and the proposed dynamic droop is applied as illustrated in Figure 2c (dotted lines) and (d). In this case, once the voltage $E_{i,inv}$ exceeds the initial dynamic lower limit $E_{i,LO}$, IBR_i does not enter the droop mode (See Figure 2d) as in the IEEE std. fixed setting case. Instead, $E_{i,LO}$, starts dynamically to increase and heading the $E_{i,inv}$ by a predefined small margin. This allows the IBR_i to continuously operate outside the droop mode and injects $P_{i,inv}$ based on the available sun power (without curtailment) as long as $E_{i,inv}$ remains below the maximum dynamic lower limit (Max_{DY-LO}). As illustrated in Figure 2d, while the power $P_{i,inv}$ continued to increase (even after the time t_c due to the dynamic droop), the voltage $E_{i,inv}$ started to fall before exceeding the maximum dynamic lower limit (Max_{DY-LO}). This gives an indication that the injected power $P_{i,inv}$ is not responsible for the voltage rise and not utilizing this available sun power impacts unfairly IBR_i. In contrast, using a fixed setting results in unfairly losing up to 50% of the available sun power as shown in Figure 2a.

2.2.2 | A case when the IBR's injected power is responsible for the voltage rise

Figure 3 illustrates a comparison of the fixed and dynamic settings when the injected power $P_{i,inv}$ is responsible for the voltage rise. The results of using IEEE std. fixed setting is shown in Figure 3a. In this case, the IBR_i enters the droop mode at t_{oo} and both $E_{i,inv}$, $P_{i,inv}$ continue to increase during the time interval t_{oo} to t_{co}. The curtailment takes place after t_{co} when $P_{i,sun} \geq P_{i,inv}$ and the operating point (E_i, P_i) is settled between the low break-out ($E_{i,LO}$) and the high break-out ($E_{i,HI}$) as shown in Figure 3a. The time interval from entering the droop mode (t_{oo}) to starting curtailment instant of fixed setting (t_{co}) may take minutes or hours based on the system conditions and available sun power.

When applying the dynamic droop, in which the initial lower limit ($E_{i,LO}$) is set to be heading $E_{i,inv}$ by a predefined percentage ($E_{i,LO} = (\beta\%)\ E_{i,inv}$) is shown in Figure 3b. Unlike the previous case (case A), the voltage $E_{i,inv}$ continued to increase with the injected power while the droop is delayed (due to increasing $E_{i,LO}$). However, when $E_{i,LO}$ exceeds its maximum dynamic low-limit ($E_{i,LO} > Max_{DY-LO}$) at time t_{o1} as shown in Figure 3b, and the IBR_i enters the droop mode. It can be concluded from this case that the continuous increase in the injected power $P_{i,inv}$ forced the IBR_i voltage $E_{i,inv}$ to increase beyond the Max_{DY-LO} and this IBR_i is categorized as responsible for a voltage rise. The inverter IBR_i limits this voltage rise to exceed the standard limit. As it enters the droop mode at t_{o1}, curtailment takes place after t_{c1} when $P_{i,sun} \geq P_{i,inv}$ at which the operating point (E_i, P_i) is settled between the maximum dynamic low-limit (Max_{DY-LO}) and the high break-out ($E_{i,HI}$) as shown in Figure 3b. The difference in the time interval t_{co} to t_{c1} represents additional time duration provided by the dynamic setting for IBR_i (responsible for the voltage rise) to use fairly the available sun-power before curtailment takes place.

3 | SYSTEM MODEL AND OPERATION ASSUMPTIONS

Figure 4a shows a typical local-area DN with a defined x-y coordination of all system components. This network is simulated in PSCAD and used to test and validate the proposed algorithms. The DN has an 11 kV switching station (SWS) connected to the utility system and supplies distribution substation in a radial configuration. The local area DN has 13, 11/0.4 kV distribution substations (SS1 − SS13), each substation supplying 0.4 kV

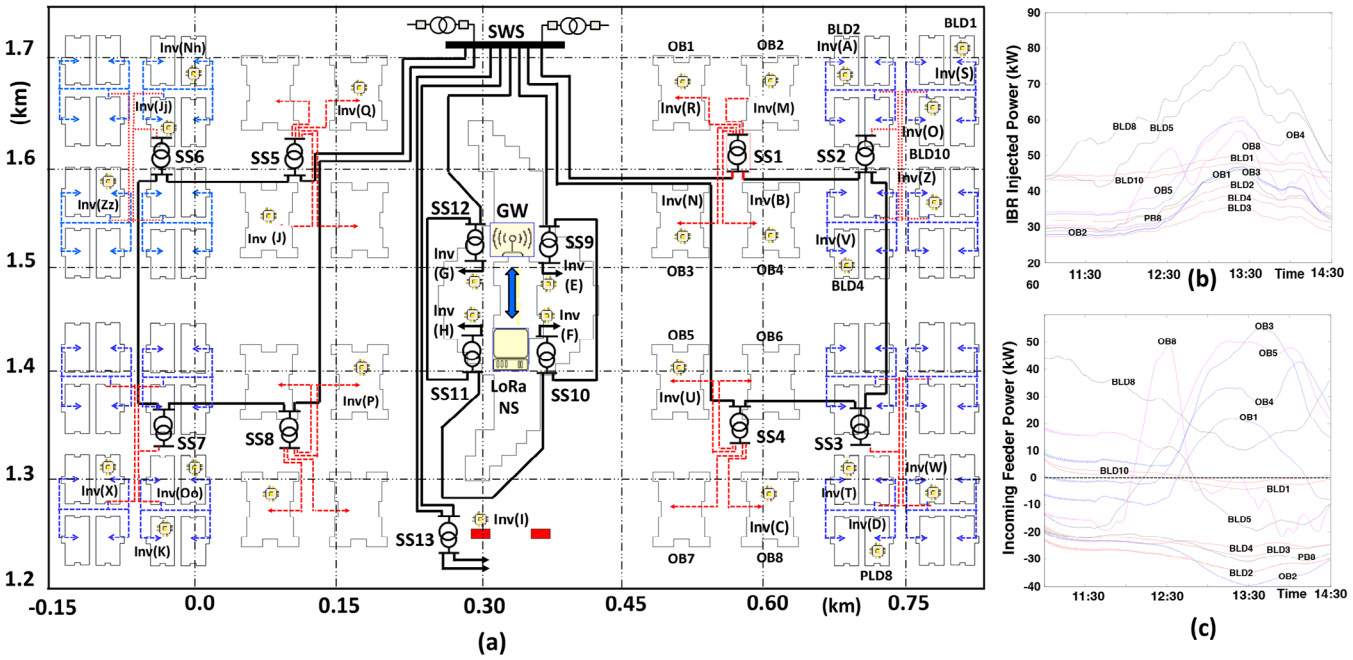

FIGURE 4 (a) A typical local-area DN, (b) the injected power from IBRs connected to SS1–SS4 and (c) the power in the feeders from distribution substations SS1–SS4 to loads.

end-users (EU) customers directly or through pillar boxes (PBs). There are 86 EU customers of different classes and different load profiles. Among those 86 EUs, 29 have IBRs rated at 0.4 kV. All the IBRs (labeled as A, B, … etc.) have LoRaWAN communication capability and report to LoRa Network Server (LoRa-NS) through a gateway (GW) as illustrated on the system model in the figure.

The higher layer of Figure 4a shows the LoRaWAN system model with x-y coordinates of all 29 IBRs' sensing nodes, a single GW, and LoRa-NS. The topology is assumed as "star-of-stars" for a coverage area of 0.55 km^2 (1.0 km × 0.55 km). All IBRs are located within the transmission range of the GW at the center of the DN. The LoRa-NS, located close to the GW, manages the settings of all IBRs and defines the boundary of a dynamic cluster. The IBRs are configured with similar spreading factors (initially SF = 7) and transfer powers (TP = 14 dBm).

Samples of 14 IBRs injected power during the sun peak interval (11 am–2:30 pm) are presented in Figure 4b. The power flow (and its direction) in each feeder connecting the distribution substations (SS1–SS4) to the EU-customers with IBRs is shown in Figure 4c. All IBRs' low and high break-out settings are selected according to IEEE std. 1547 (1.05–1.10 pu). These loads and IBRs are used as a reference to justify the usefulness of the proposed algorithm in fair utilization of IBRs and voltage control.

The following assumptions are considered in this paper:

1. The proposed algorithm is implemented during the duration where the available sun-power has high values that drive the IBRs to operate in the droop control mode ($E_{i,LO} \leq E_i \leq E_{i,HI}$). The time-duration for this condition is assumed as 11:00–14:30.
2. All IBRs in the local-area DN are assumed to be able to report to the LoRa-NS (up-stream/down-stream messages) during a specified reporting-time-interval, which has been defined based on LoRaWAN communication time requirement; 120 s as a worst-case scenario is assigned for this interval and the voltage/load profiles are assumed constant.
3. Fairness for IBRs means that to allow them to utilize the maximum available sun-power and only those with a significant contribution to substation voltage violation will be clustered and penalized by controlling their injected power. The violation responsibility is changing as the load, available sun-power, or system configuration change, hence IBRs in a cluster are continuously changing (dynamic cluster) based on a quantifying measure of IBRs mutual sensitivity.
4. This study is mainly concerned with the active power impact of IBRs assuming distribution networks with large R/X ratio where the reactive power impact can be ignored. This study assumes IBRs in distribution networks have a negligible reactive power capability.
5. The LoRaWAN communication challenge can be overcome by selecting other communication media for real-time application and a more secure environment. This challenge is accepted to benefit the stand-alone communication system that allows a 3-party involvement in the business of the energy market.

4 | LORAWAN COMMUNICATION SYSTEM

LoRaWAN is a cost-effective, license-free platform that uses scientific and medical (ISM) band. It is easy to deploy, manage,

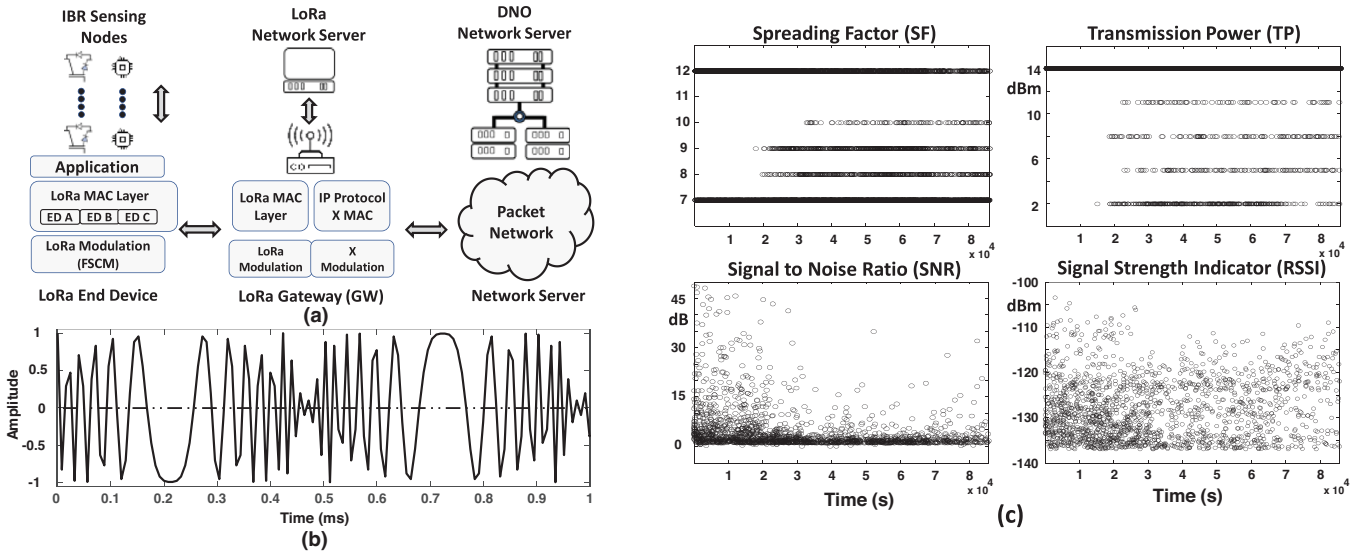

FIGURE 5 (a) The schematic diagram of LoRa architecture, (b) simple realization of the FSCM for one symbol and (c) OMNeT++ simulation results of LoRaWAN parameters (SF, TP, SNR and RSSI).

and suitable for energy service aggregators, especially in areas lacking 5G coverage or requiring extensive device deployment. LoRaWAN offers extended coverage up to 15 km, trading off with a reduced data rate of about 0.3 kilobits per second.

In the envisioned system, depicted in Figure 4, LoRaWAN facilitates the transmission of information from LoRa end devices (IBRs sensing nodes) to gateways (GWs) situated several kilometers away, all while maintaining low energy consumption. These GWs, in turn, efficiently relay the messages from IBRs sensing nodes to the LoRa network server using standard interfaces like 4G modems or Ethernet, as demonstrated in [19]. The IBRs sensing nodes exhibit the capability to communicate directly with each other or through the GWs, offering versatility in network interactions.

Figure 5a provides a schematic overview of the LoRa architecture, showcasing its sublayers. The IBRs, functioning as sensing components, reside at the application sublayer. The LoRa media access control (MAC) sublayer governs the transmission, reception, and channel-sensing behavior of devices. This MAC sublayer is meticulously crafted to enhance the probability of successful message delivery while minimizing power consumption. The specific MAC protocol employed is contingent upon the class of operation of the IBR-sensing parts, categorized as A, B, or C. The application uses the 868 MHz ISM band with 125 kHz bandwidth for LoRaWAN in Europe. It employs Frequency Shift Chirp Modulation (FSCM) in the physical layer, offering a trade-off between data rate and coverage area through the spreading factor (SF).

Figure 5b illustrates a straightforward representation of FSCM for a 7-bit symbol [1001011] with SF set to 7, providing a visual insight into the modulation process. LoRaWAN's time-duration limit for messages is compatible with various distribution network applications. The IEEE standard allows 0.5−60 s for IBR active power changes in response to voltage changes, with a maximum response time of ≤30 s to requests.

OMNeT++ (object-oriented modular discrete event network), a FloRa-module simulator [40] based on the INET framework [41] is used to simulate the LoRaWAN DN model. The OMNeT++ simulator allowed the modeling of the LoRa network and its communication protocols. The simulation results presented in Figure 5c were conducted independently of the power system simulations with the aim of evaluating the performance of the LoRaWAN as a communication platform. As shown in Figure 5c, an adaptive data rate (ADR) scheme is activated to optimize the SFs (two cases with initial SF = 7, 12) and the transmission power (initial TP = 14 dBm) and hence managing data rates for each ED-IBR individually. The ADR implementation enables IBRs in proximity to gateways to utilize lower spreading factors and achieve higher data rates compared to more distant devices. All simulation scenarios have a signal-to-noise ratio (SNR) above 0 and a received signal strength indicator (RSSI) between −135 dBm and −110 dBm.

5 | MUTUAL SENSITIVITY CLUSTERING-BASED APPROACH

The clustering of distribution networks offers an effective approach for coordinating and controlling large numbers of end users' smart inverters (EU-IBRs). In such applications, the efficacy of clustering relies on the accurate capturing of how strongly two nodes are mutually coupled and to what extent a change in a node's power-voltage interaction may impact the parameters of the other coupled nodes.

In the proposed application, the mutual coupling between nodes (i, j) is monitored and estimated based on the sensitivity of these nodes to the rate of change of the node voltage with respect to the power $(\partial E_i/\partial P_j)$. Based on the sensitivity level, the IBRs to be included in the system clusters are defined. Several methods have been previously proposed in the literature

to define a cluster boundary of sensitive coupled nodes (e.g. [42–44]). However, the key observation regarding these methods is their tendency to form static clusters as well as their oversight in considering the influence of the injected power from IBRs, despite the IBRs' power remains the principal factor in voltage regulation management. As the penetration level of IBRs continues to rise, the intermittent nature of the IBR's injected power can significantly impact the voltage at the coupled nodes as well as the overall voltage profile at the system level. To effectively capture those impacts when managing voltages, it becomes essential to incorporate the IBRs' dynamics into the sensitivity analysis of network voltages. Specifically, in regulating network voltages with IBRs, it is crucial to account for the sensitivity of IBR-injected power (as opposed to bus power) to bus voltages which ensures a more comprehensive approach to manage the IBRs for voltage regulation. It should be noted that, when considering the sensitivity of IBRs' injected power to voltage for clustering a network, clustering becomes dynamic. This dynamic clustering approach enables a more efficient way of managing the increased penetration level of IBRs, thus facilitating more effective voltage regulation strategies. Hence in this paper, an effective dynamic mutual sensitivity approach is proposed which leads to a dynamic system clustering method. This method integrates distributed IBRs and LoRaWAN technology to continuously define the changing sensitivity levels among coupled nodes and update the cluster boundary by including only IBRs that have the most significant impact on voltage levels in DNs. The proposed mutual-sensitivity dynamic clustering method in this paper aims to control DN node voltages, use the most available sun power, and satisfy IBRs utilization fairness. The subsections below explain the proposed mutual-sensitivity algorithm and its implementation to achieve dynamic clustering in DN.

6 | INTRODUCTION TO ELECTRIC DISTANCE AND VOLTAGE-POWER SENSITIVITY

The concept of electrical distance between two nodes is used to quantify the voltage sensitivity to power among different nodes. This electric distance is extracted from the Jacobian or the system's bus impedance [45]. Based on the Jacobian matrix, the voltage-power relationship is given as

$$\begin{bmatrix}\Delta P\\ \Delta Q\end{bmatrix} = [\mathrm{J}]\begin{bmatrix}\Delta\delta\\ \Delta E\end{bmatrix} = \begin{bmatrix}J_1 & J_2\\ J_3 & J_4\end{bmatrix}\begin{bmatrix}\Delta\delta\\ \Delta E\end{bmatrix}, \tag{7}$$

where [J] is the Jacobian matrix, the elements of which J_1, J_2, J_3, and J_4 are sub-matrices representing the sensitivity of active power to the changer in power angle ($\partial P/\partial\delta$), the sensitivity of active power to the change in bus voltage ($\partial P/\partial E$), the sensitivity of the reactive power to the change in the change in power angle ($\partial Q/\partial\delta$), and the sensitivity of the reactive power to the change in bus voltage ($\partial Q/\partial E$), respectively.

Unlike using the reactive power to derive the voltage sensitivity as in [45], in this paper, the sensitivity to active power ($\boldsymbol{R^P}$) is as follows.

$$\boldsymbol{R^P} = \left(J_2 - J_1 J_3^{-1} J_4\right)^{-1}, \tag{8}$$

$$R^P_{jj} = \frac{\partial E_j}{\partial P_j}\ R^P_{ij} = \frac{\partial E_i}{\partial P_j}, \tag{9}$$

$$\alpha_{ij} = \frac{R^P_{ij}}{R^P_{jj}}, \tag{10}$$

where α_{ij} is defined here as the active power-based mutual sensitivity between buses i and j.

6.1 | The proposed IBRs active power-based mutual sensitivity (APMS)

When an inverter at bus j is set to operate at its power droop mode, the relationship between the voltage (E_j) and the injected power (P_{inv}) is given by a linear equation as

$$E_j = mP_{inv} + C, \tag{11}$$

where m is the slope of the droop and C is a constant. The voltage sensitivity to the injected active power in a network with inverters can be estimated by defining $R^P = \partial E/\partial P$. Then, using (9) and (10), the degree of the sensitivity (mutual sensitivity) of voltage coupling between two buses j and i with inverters is represented as

$$\alpha_{ij} = \frac{R^P_{ij}}{R^P_{jj}} = \frac{\partial E_i/\partial P_j}{\partial E_j/\partial P_j}\ or\ \alpha_{ij} = \frac{\partial E_i}{\partial E_j}. \tag{12}$$

When two inverters are set to operate in the droop mode at buses i and j, then their voltage sensitivities to active power can be represented in terms of the linear equation (11) and hence:

$$\alpha_{ij} = \frac{\partial\left(m_i P_{inv,i} + C_i\right)}{\partial\left(m_j P_{inv,j} + C_j\right)}. \tag{13}$$

Equation (13) can be simplified to:

$$\alpha_{ij} = \left[m_i/m_j\right] * \left[\Delta P_{inv,i}/\Delta P_{inv,j}\right]. \tag{14}$$

Clearly (14) illustrates how the sensitivity of voltage to active power at a bus j is influenced by the inverters' injected power (ΔP_{inv}) and the slope of their droop (m) while operating in the droop mode. This visualization serves to demonstrate the effect of the slope on sensitivity.

When an inverter operates in the droop mode, the operating point (E_i, P_i) is altered while keeping the slope unchanged. This alteration can be accomplished by shifting the low and high break-out values (i.e. shifting $E_{i,LO1}$ to $E_{i,LO2}$ and $E_{i,HI1}$ to $E_{i,HI2}$ as shown in Figure 6a). The inverter is compelled to function at different operating points while the slope remains

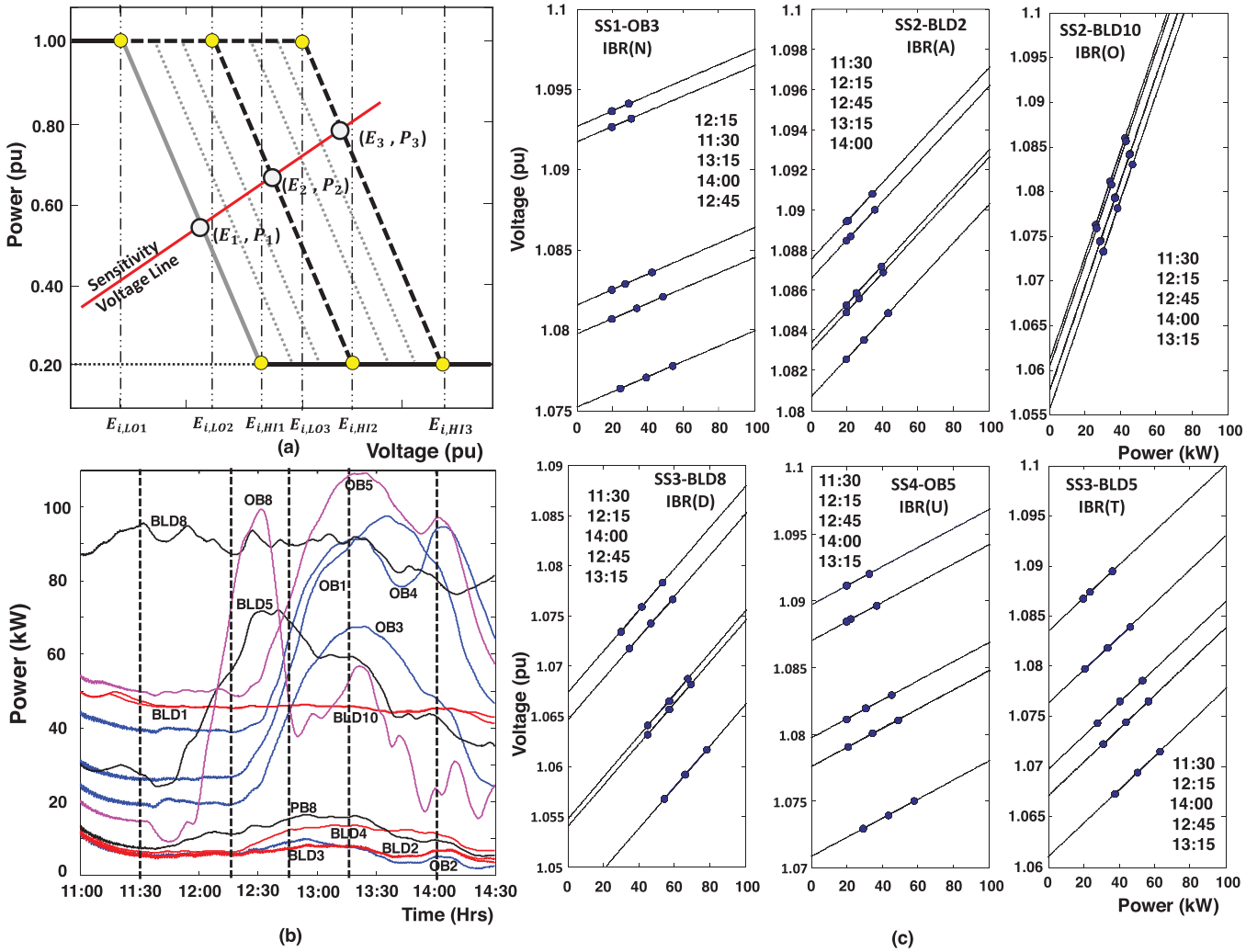

FIGURE 6 (a) Inverter droop at different high and low break-out values, (b) the connected load power (kW) for 14 customers having IBRs indicating the five measurement instants, and (c) measured sensitivity lines at 5 time-instants for 6 inverters.

constant. These operating points are used to generate the sensitivity voltage line as illustrated in Figure 6a. In practice, each inverter is configured to operate at different low and high settings ($E_{i,LO}$, $E_{i,HI}$), and different measurements are reported through LoRaWAN in order to develop the voltage sensitivity line. This process is illustrated below based on the distribution network shown in Figure 4.

In order to monitor and estimate the voltage self-sensitivity to active power at designated buses ($R^P = \partial E_j / \partial P_j$), the 14 IBRs connected to SS1–SS4 in the system of Figure 4a are considered in developing voltage sensitivity lines. The results of these voltage sensitivity lines are conducted where all IBRs are assumed to have a rating of 100 kW, and their injected power varies with time as illustrated in Figure 4b while the connected loads range from 5.0 to 110 kW as shown in Figure 6b.

Samples of the voltage sensitivity lines from six IBRs connected to 4 substations are shown in Figure 6c. To emphasize the changes in the available sun-power and the connected load, the measurements take place at five different time instants (11:30, 12:15, 12:45, 13:15, and 14:00) as marked by vertical lines in Figure 6b. The IBRs are set to operate according to IEEE std. settings under three different droop conditions (1.05–1.1, 1.04–1.09, 1.03–1.08 pu) as shown by the dotted points in Figure 6a. As the sun-power and load vary, the operating point (E_i, P_i) changes and new voltage sensitivity lines are generated accordingly. The voltage sensitivity lines and their appearance time-instant-sequence, sorted from high to low, are illustrated in Figure 6c.

It is apparent from these results (while operating in the droop mode) that the sensitivity relationship between voltage and power ($R^P = \partial E_i / \partial P_i$) can be effectively linearized and modeled, maintaining a consistent slope across different droop settings and at different time instants.

Based on this constant slope, a voltage sensitivity line can be modeled and used to estimate (E_i, P_i) as a setting change. This reduces the reporting time requirement of LoRaWAN considering all daily time instants. Hence after the initial complete reporting of the settings at a certain time instant, the voltage

sensitivity line is developed, and only one (E_i, P_i) should be reported and used with the fixed slope to develop the other voltage sensitivity lines at new time instants.

The slops of the voltage sensitivity lines are used to estimate the active-power mutual sensitivity reference index as indicated in (14). This index is generated while the inverter is set to operate in the droop mode using different IEEE std. settings (1.05–1.1, 1.04–1.09, 1.03–1.08 pu). While the slopes of the voltage sensitivity lines are constant, the location of these lines changes with time, system condition, and inverters injected powers ($\Delta P_{inv,i}$ and $\Delta P_{inv,j}$). The impact of these changes is considered by normalizing α_{ij} to the ratio $[P_{inv,i}/P_{inv,j}]$. This ratio is selected while all the DN inverters operate at 1.05–1.10 pu setting. Hence the $APMS_{ij}$ reference index of the voltage sensitivity of all DN buses to the change in the injected active power in bus j is estimated as

$$\boldsymbol{APMS_{ij}} = \frac{[(\boldsymbol{m_i}*\boldsymbol{\Delta P_{inv,i}})/(\boldsymbol{m_j}*\boldsymbol{\Delta P_{inv,j}})]}{[\boldsymbol{P_{inv,i}/P_{inv,j}}]}, \quad \textit{for } i = 1, 2, 3, \ldots\ldots n \tag{15}$$

where n is number of inverters in a DN. The reference index is generated at different time instants and updated based on the $[P_{inv,i}/P_{inv,j}]$ ratio in each time instant of the actual DN application.

It should be noted that while $P_{inv,i}$ could be influenced by multiple inverters, not just j, the application of the proposed approach is mainly for local-area distribution networks with a constrained geographical area. This limitation reduces the likelihood of significant, uncorrelated changes in intermittent resources (sun), or end-user loads across the network. This assumption ensures that temporary, minor changes between reporting intervals do not significantly disrupt the calculations of mutual influence. This ensures that only relevant interdependencies are captured, and unrelated changes are excluded from the calculation.

For a DN with n IBRs, the $APMS$ among all IBRs is

$$\boldsymbol{APMS} = \begin{bmatrix} APMS_{11} & \cdots & APMS_{1k} & \cdots & APMS_{1n} \\ APMS_{21} & \cdots & APMS_{2k} & \cdots & APMS_{2n} \\ \vdots & & \vdots & & \vdots \\ APMS_{i1} & \cdots & APMS_{ik} & \cdots & APMS_{in} \\ \vdots & & \vdots & & \vdots \\ APMS_{n1} & \cdots & APMS_{nk} & \cdots & APMS_{nn} \end{bmatrix} \times \begin{bmatrix} P_k/P_1 & 0 & 0 & 0 & 0 & 0 \\ 0 & P_k/P_2 & & 0 & 0 & 0 \\ 0 & & .. & 0 & 0 & 0 \\ 0 & & & P_k/P_k & 0 & 0 \\ 0 & 0 & 0 & 0 & .. & \\ 0 & 0 & 0 & 0 & 0 & P_k/P_n \end{bmatrix}. \tag{16}$$

At time instant t, a reference $APMS_{REF}$ can be estimated in terms of the unit matrix [U], a fixed mutual sensitivity matrix $[APMS_{ij}]$, and an updating factor $[P_{inv,j}/P_{inv,i}]$ column matrix as follows.

$$[APMS_{REF}] = [P_{inv,j}/P_{inv,i}]\,[\mathrm{U}]\,[APMS_{ij}]. \tag{17}$$

Initially, the column matrix $[P_{inv,j}/P_{inv,i}]$ is measured based on IEEE std., setting of 1.05–1.10 pu. As time changes, the load and sun-power change and a new reference of $APMS_{REF}$ is generated by updating $[P_{inv,j}/P_{inv,i}]$ ratios based on LoRaWAN reported and modeled data at that new time instants.

The Sensitivity Contribution of an IBR at bus k (SC_k) to all other IBRs in the DN is estimated by updating the column matrix $[P_{inv,k}/P_{inv,i}]$ while IBRs operate at the default dynamic setting and then compute the norm as

$$SC_k = ||[P_{inv,k}/P_{inv,i}][APMS_{REF}]|| \textit{ for } i = 1, 2, 3, \ldots\ldots n. \tag{18}$$

The sensitivity contribution (SC_k) is a dynamic parameter which can be used to identify the most sensitive IBRs that have a significant contribution to voltage variation. Its concept is used to define dynamic clustering as it will be discussed in Section 5.4.

6.2 | Validation of the proposed mutual sensitivity measurement approach using the voltage sensitivity lines

To validate the proposed mutual sensitivity measurement approach, the sensitivity of active power to bus voltages, (i.e. α_{ij} in (12)) was evaluated through two approaches. First, it was calculated using the conventional Jacobian matrix method, (derived from network impedance parameters and load flow analysis), which served as a benchmark for comparison. Subsequently, α_{ij} was determined using voltage sensitivity lines described in the previous section. Given that APMS is primarily calculated based on α_{ij} (by normalizing α_{ij} as described in (15)), this comparison directly assesses APMS's accuracy. While APMS calculates α_{ij} based on measured inverters' responses, the Jacobian matrix derives α_{ij} from network parameters and used as a benchmark for comparison. Thus, to validate APMS, the measured α_{ij} values are compared against those obtained from the Jacobian matrix. This comparison assessed the accuracy of the measured α_{ij}, thereby confirming the validity of APMS.

This comparative analysis was conducted on a single feeder with five buses equipped with five IBRs. The details of the feeder are shown in Figure 7a. When calculating α_{ij} using the proposed approach, two operation condition are considered: all IBRs injecting power at full capacity (100%), and IBRs functioning at 50% capacity. The results of those two cases are compared with the Jacobian-based approach as shown in Figure 7b (each group of bars indicates the sensitivity of a bus to the remaining buses in the feeder). The results demonstrate that the proposed approach for measuring the sensitivity achieves comparable accuracy to the Jacobian approach while eliminating the need for load flow analysis and system parameter calculations. It should be emphasized that the accuracy of the proposed approach stems from the direct measurement of voltage sensitivity. Although network parameters are not explicitly required, their influence is indirectly reflected in the measurements, making the proposed approach comparable to the Jacobian method. This measurement-based approach makes the proposed approach applicable to any distribution network;

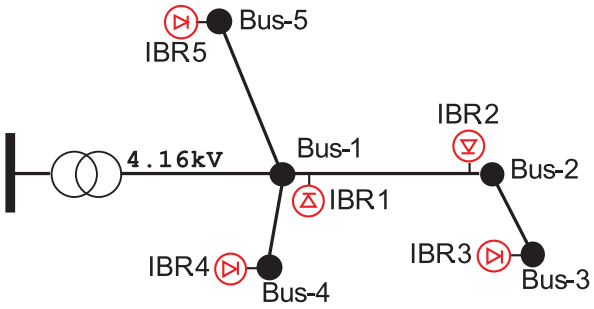

Line impedance

z12 = 0.380 Ohms, 3.2494 mH
z23 = 0.246 Ohms, 1.1662 mH
z14 = 0.246 Ohms, 1.1662 mH
z15 = 0.943 Ohms, 3.5386 mH

(a)

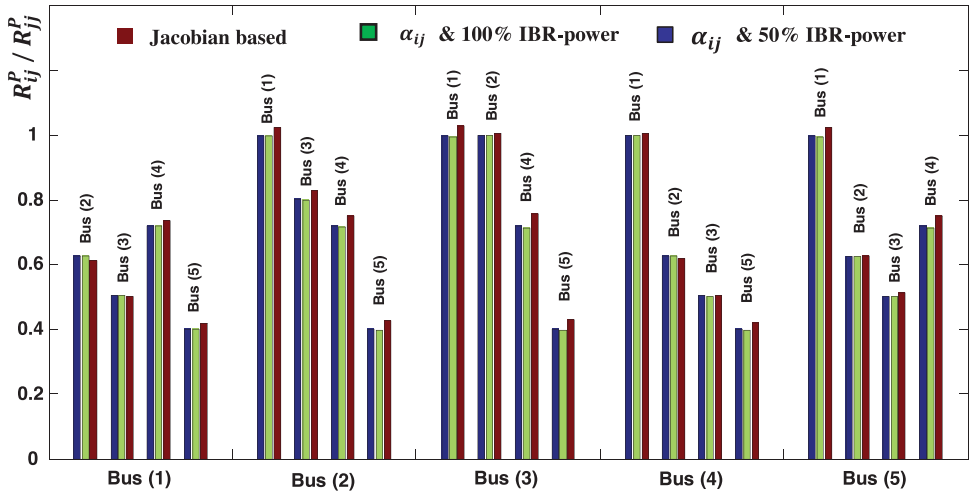

(b)

FIGURE 7 (a) A 5-bus test distribution network, and (b) comparison between the proposed sensitivity measurement approach and Jacobian based sensitivity calculations.

however, the accuracy of the measurement may be impacted in weak networks.

The value of α_{ij} is then used to calculate the active power mutual sensitivity (APMS) as discussed in the previous subsection. It should be noted that, unlike the concept of electrical distance where $D_{ij} = D_{ji}$, in the proposed APMS, the active power-based mutual sensitivity between any two buses i and j results in $APMS_{ij} \neq APMS_{ji}$. This shows a distinct sensitivity of each bus (or IBR), indicating that the voltage sensitivity of bus j due to a change in power at bus i differs from the voltage sensitivity of bus i due to a change in power at bus j. This unequal relation reflects the logical impact of the non-equal IBR injected power into the two buses i and j beyond the impact of the power flow in the lines and/or the system line impedances. Hence the proposed APMS method provides significant insights into the sensitivity of voltage at various buses.

Furthermore, the active power-based mutual sensitivity $APMS_{ij}$ shows a significant contribution (quantified with SC_k) to the adjacent IBR-buses connected to the same substation while moderate or low contribution to other IBR-buses connected to different substations. However, the contributions' significance changes over time as the load, sun-power and/or system substation feeders' configuration change. This means if an IBR at bus k has the highest contribution at a certain time instant, it may have a lower contribution at another time instant or another system configuration.

6.3 | Dynamic clustering based on mutual sensitivity

Clustering of DNs with a large number of smart inverters offers an effective approach for system management, optimal and fair

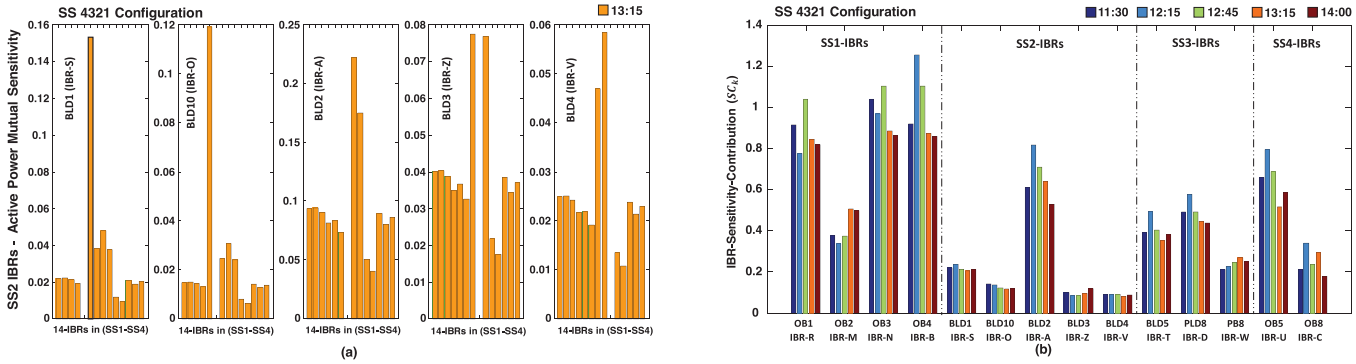

FIGURE 8 (a) Mutual sensitivity for SS2 5-IBRs to all other 14-IBRs, IBRs, and (b) IBR sensitivity contribution of all 14-IBRs during 5-time instants and substations configuration 4321.

operation of IBRs. The proposed clustering method considers load-classes of different sizes and distributed energy resources (IBRs) to develop a dynamic voltage-power sensitivity model and utilize it to define a dynamic cluster boundary. The proposed algorithm sets all IBRs in the DN to operate initially at the dynamic setting (default setting) without any cluster. Dynamic clustering is triggered only in case of substation voltage violation as reported by the DNO-NS to LoRa-NS. The dynamic cluster approach considers only the most sensitive IBRs that have a significant contribution to voltage violation to include in the developed cluster boundary. The cluster boundary and the number of IBRs continuously change as the sun-power, loads and IBR mutual sensitivity change.

The concept of APMS in (17) and SC_k in (18) are used to develop a dynamic cluster model that continuously varies with time based on DNO-NS and LoRa-NS events and scheduled voltage-power interaction information. The proposed dynamic clustering model guarantees that the most sensitive IBRs that have a significant contribution to voltage limit violation are included in this cluster. The clustered sensitive IBRs located at strongly coupled buses are then used in the voltage regulation process without involving (unfairly) the non-sensitive IBRs nodes.

A sample of the reference index of the active power mutual sensitivity ($APMS_{ij}$) for SS2 five IBRs to all the fourteen IBRs in the DN are shown in Figure 8a. These measures are generated using (15) during the peak load time at 13:15. The $APMS_{ij}$ are changing with time as the load and available sub-power change.

The cluster boundary is dynamically developed and updated based on the sensitivity contribution (SC_k). Figure 8b shows the SC_k of the 14-IBRs and the variation in their sensitivity contribution during 5 time-instants (11:30, 12:15, 12:45, 13:15, and 14:00). The sensitivity contributions SC_k is used to define the most sensitive IBRs and their dynamic nature is monitored by the variation in their values with time. For example, in SS1, IBR-N (OB3) has the highest SC_N at 11:30 time-instant while IBR-B (OB4) SC_B has the highest contribution at 12:15 (see the dark and light blue bars for SS1-IBRs in Figure 8b). The change in the significance of the contribution comes from the updating column matrix $[P_{inv,k}/P_{inv,i}]$ in (18) which reflects the continuous change in the load, sun-power, and injected IBR-power at that time instant. Based on the location of the substation with voltage violation, one or more of the IBRs with the highest SC_k are selected to include in the dynamic cluster.

7 | THE ROLE OF LORAWAN COMMUNICATION IN DYNAMIC CLUSTERING AND SETTINGS

Dynamic settings and dynamic clustering rely on LoRaWAN scheduled communication at the IBRs sensing nodes as well as DNO-NS and LoRa-NS event-based communication as illustrated in Figure 5. The DNO-NS and LoRa-NS communication media can be provided with high-reliability. The LoRa-NS and IBR sensing nodes communication form an opportunity to engage a third party (with a stand-alone communication system) in the energy market. However, this communication provides different challenges in terms of transmission time, coverage distance, high interference, and high probability of packets' collision.

In this application, the FSCM is used and the proportion of transmitted bits that actually carry information (coding rate, CR) of 4/5 is assumed. Theoretically, for a 7-bit symbol, SF of 7, and a bit rate of 5.5 kb/s, the minimum time required to submit one symbol is 1.273 ms, and the coverage distance can reach up to 2.0 km. This coverage is fairly adequate for a DN local area network and covers the whole local area DN shown in Figure 4. However, as the SF is increased to 12, the bit rate is reduced to 293 b/s and the time required to send one symbol (12 bits) is 40.96 ms, for a higher coverage distance of 15.0 km.

It has been recommended in [30] to use a duty-cycle of 1% per sensing node to manage high interference as well as a high probability of packets' collision. This means that it is allowed for each IBR sensing node to transmit only 36 s per 1 h. Assuming that the payload of the electrical measurements consists of 8 bytes, this means a transmission time (air-time) of about 56.6 ms (with SF = 7 and BW = 125 kHz) [31]. This time includes 13 bytes used for controlling the transmission and other standard-related factors. For a 1% duty cycle, this IBR sensing node is

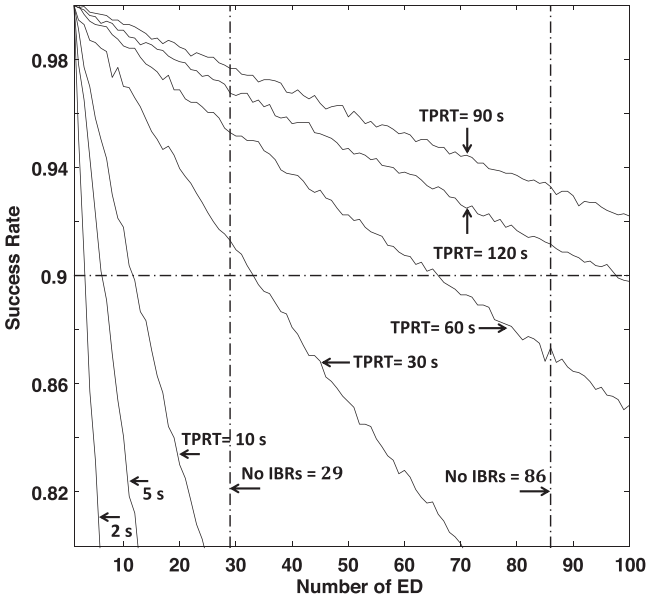

FIGURE 9 The transmission time and the success rate.

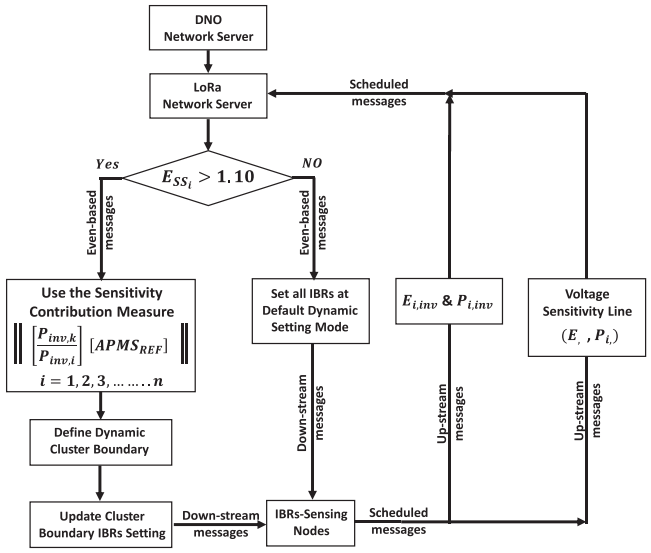

FIGURE 10 A flowchart of the proposed dynamic clustering and setting algorithm.

allowed to transmit more than 600 times per hour. Hence, this duty cycle restriction is not a problem for the application given in this paper.

Monte-Carlo simulation is used considering different parameters to investigate the time requirements of the proposed algorithm. The success rate of transmission considering 100 IBR sensing nodes is shown in Figure 9. The air-time required by each IBR is assumed 100 ms. IBRs have a total period of random transmitting (TPRT) that varies between 2 s and 120 s. A large improvement is achieved in the success rate as the TPRT is increased. For 29 IBRs as distributed in Figure 4, the success rate is more than 90% for TPRTs > 25 s. If all the customers in the DN system have IBRs (IBRs = 86), the success rate is more than 90% for TPRTs > 80 s.

For 29 IBRs, considering the worst-case scenario, where all sensing nodes messaging the LoRa-NS at the same time. The average required uplink time is 25 s for a 90% success rate (see Figure 9), downlink time (3 s, assuming no collusion as the GW manages downlink messages transmission), and a processing time (assumed 8 s) in LoRa-NS. Then considering the worst-case scenario, a rough estimate of the total required time of updating all IBRs settings is around 40 s.

The flowchart of Figure 10 summarizes the implementation procedure of the proposed dynamic setting and clustering method. The scheduled messages are used under normal operation condition (NOC) to form the voltage sensitivity lines and generate $[APMS_{REF}]$ and SC_k as in (15) and (16). Furthermore, the scheduled messages assign default dynamic settings among all IBRs, during NOC, that assure maximum utilization of available sun-power. The process is explained as follows:

- During NOC, the LoRa-NS receives a scheduled upstream message (E_i, P_i) in a sequential order from all IBRs to form voltage sensitivity lines. The initial voltage sensitivity line is generated from the upstream messages of (E_i, P_i) during IEEE std. settings of 1.05–1.10, 1.04–1.09 and 1.03–1.08 pu. For the other time-instants, the voltage sensitivity lines are generated from scheduled upstream messages (E_i, P_i) at one setting (1.05–1.10 pu) and then the constant slop of the initial voltage sensitivity line is used to estimate (E_i, P_i) for other settings. These scheduled upstream messages are used to estimate the active power mutual sensitivity matrix $(APMS_{ij})$ among all IBRs and define its sensitivity contribution (SC_k).
- During NOC, all the DN IBRs are set to operate on the proposed dynamic setting mode (default setting) without any cluster. A fixed value is assigned to the high break-out limit $(E_{i,HI})$ and a dynamic (not fixed) low break-out $(E_{i,LO})$ with predefined Min_{DY-LO} and Max_{DY-LO}. During NOC the dynamic $E_{i,LO}$ is continuously heading the IBR voltage $(E_{i,inv})$ by a small percentage $(\beta\%)$ constrained by Max_{DY-LO} of 1.095 pu and 1.10 pu violation limit. The aim of increasing low break-out $(E_{i,LO} \leq Max_{DY-LO})$ is to examine the responsibility of IBRs to voltage rise and to allow them to use fairly the maximum available sun-power without violating the substation voltage standard limit. Using (1)–(4), the IBRs continuously update their dynamic settings based on the time-instant load and available sun-power.
- The event-based messages between DNO-NS and LoRa-NS are triggered under abnormal operation condition (AOC). These messages are used to select IBRs based on SC_k and develop dynamic clusters with updated dynamic settings. Only the selected IBRs in the dynamic clusters update their dynamic settings to regulate substation voltages without unfairly penalizing non-responsible IBRs by involving them in the curtailment process.
- During AOC, the DNO-NS initiates the dynamic clustering process by sending an event-based message to LoRa-NS of the substations' buses having possible voltage violation $(E_{SS_i} > 1.10)$.

- The LoRa-NS initiates the dynamic cluster boundary by including the IBRs having high SC_i and connected to the violated substations. Based on the severity of the voltage violation, the dynamic cluster might include one or more of the IBRs with high SC_i for each violated substation.
- LoRa-NS sends an event-based down-stream message to the selected IBRs in the dynamic cluster to change their default setting. This change includes stepping down their Max_{DY-LO} and the violation limit.
- As a substation comes back to NOC, DNO-NS sends an event-based message to LoRa-NS.
- LoRa-NS sends an event-based down-stream message to exclude the IBRs related to the substation from the dynamic cluster and return to the default setting.

8 | SIMULATION RESULTS AND DISCUSSIONS

The DN model described in Section 3 is simulated using PSCAD to evaluate the performance of the proposed approach in regulating system voltages. The evaluation study focuses on customers connected to substations SS1–SS4, examining the merits of applying the proposed dynamic droop settings and dynamic clustering. Various scenarios are explored between times 11:00 and 14:30, assuming solar power availability exceeds that derived from droop control.

Five scenarios and two feeder configurations are examined to showcase the effectiveness of the proposed approach. Scenarios 1 and 3 relate to feeder configuration SS 4321 (with SS4 being the upstream substation and SS1 being the downstream substation in the 11 kV feeder). Scenarios 4 and 5 correspond to feeder configuration SS1234 (with SS1 being the upstream substation while SS4 is the downstream substation in the feeder). The settings for each scenario are provided below.

- Feeder configuration **SS 4321**; Abnormal Operation Condition (AOC):

  Scenario 1: Static cluster and fixed IEEE std. setting.
  Scenario 2: Static cluster and dynamic setting (default setting in the proposed approach).
  Scenario 3: Dynamic cluster and dynamic setting.

- Feeder configuration **SS 1234**; Normal Operation Condition (NOC):

  Scenario 4: Static cluster and fixed IEEE std. setting.
  Scenario 5: Static cluster and dynamic setting (default setting in the proposed approach).

Under configuration SS 4321, voltage violations were observed at all substations, designating this as an AOC, and thus, scenario 3 is triggered. However, under configuration SS 1234, no voltage violations occur on the substations, thus designating it as NOC. Scenario 1 (and 4 during NOC) serves as a benchmark (reference scenario) for comparison with other scenarios. The setting for scenarios 2 (and 5 during NOC) represents the default settings in the proposed approach. Further details on scenario settings are outlined in Table 1, including the summation of the percentages of power utilized by all IBRs for comparison (see Table 2 for details of the percentages).

8.1 | The impact of the proposed approach on the DN during AOC

The voltage and power responses of the IBRs during scenarios 1–3 are given in Figures 11 and 12. In Figure 11, the regulated voltage and injected power (after curtailment) by all IBRs are presented for the three scenarios. Figure 11a shows the IBRs in substations 1 and 3, and Figure 11b shows the IBRs in substations 2 and 4. In these figures, gray plots correspond to scenario 1 (the IEEE case), black plots illustrate scenario 2 (the Default), and red plots show the response during scenario 3 (with dynamic clustering). In the proposed approach, voltage monitoring at the distribution substations is continuously conducted to detect violations. However, the dynamic clustering was disabled in case of scenario (the default setting) and then enabled in scenario 3 to demonstrate its impact in managing the voltage on the distribution substation levels. The substation voltages during the three scenarios are shown in Figure 12, using the same color code for Figure 11. Below are the discussions of the responses during the three scenarios.

1. In scenario 1 (the IEEE) employs fixed low and high breakout values ($E_{i,LO}$, $E_{i,HI}$) of 1.05 and 1.10 pu, respectively. During the test time, (11:00 to 14:30), all the local voltages were regulated to less than 1.095 pu without violating the voltage at the distribution substations. All four substation voltages were less than 1.10 pu as seen in the gray plot in Figure 12. However, the total sum of the percentages of used available energy by all IBRs is calculated as 731.45% to maintain the voltage under the violation limits.
2. In scenario 2 (default setting that disables dynamic clustering), the dynamic setting is implemented on all IBRs in the substations (SS1–SS4) with $Max_{DY-LO} = 1.095$ pu. As discussed in Section 2, since the dynamic droop setting impacts only the responsible IBRs, more power has been utilized as compared to scenario 1 while maintaining the local voltages of all IBRs below the violation limits. The total sum of the percentages of used available energy by all IBRs is calculated as 1129.14%. However, during this scenario, voltage violations were observed at all the distribution substations during the time interval from 11:00 to 12:45 (see the black plot in Figure 12).
3. In scenario 3 (enable dynamic clustering), once a distribution substation voltage violation occurs, the dynamic clustering is developed based on the sensitivity contribution (SC_j). In the proposed approach, the dynamic clustering boundary is set to include two IBRs with the highest sensitivity contribution (SC_j) for each substation with a voltage violation. Based on SC_j, values in Figure 8b, initially, eight IBRs (N B A S D T U C) are included in the cluster from 11:00 to 11:25. Sub-

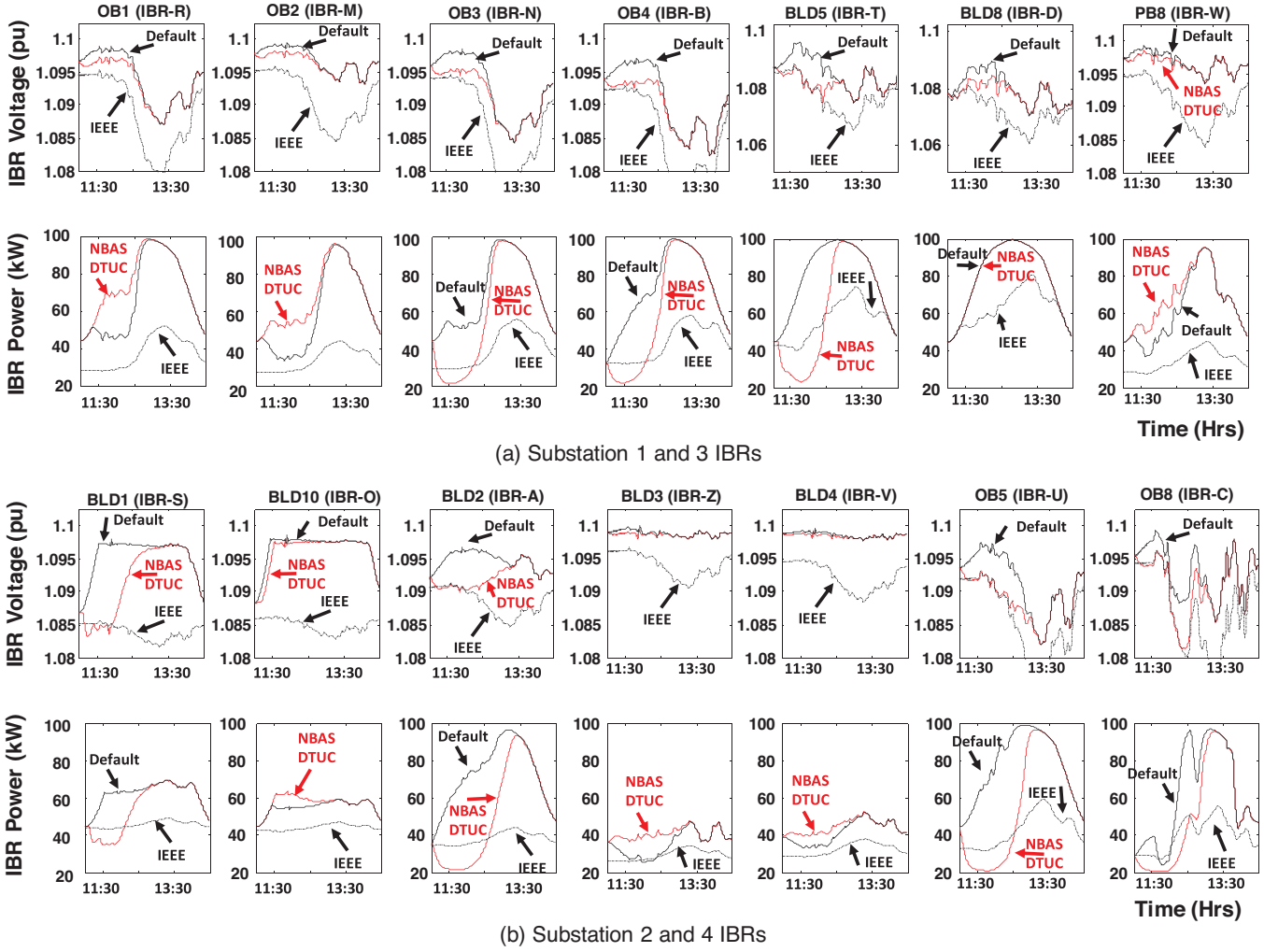

FIGURE 11 SS1 to SS4 IBRs voltages and injected powers during the operation scenarios (1)–(3) listed in Table 1.

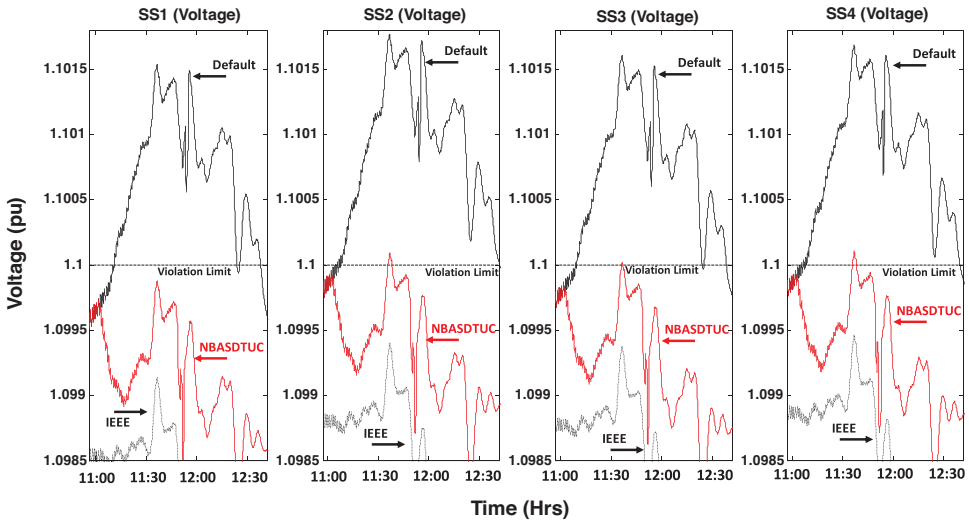

FIGURE 12 Substation voltages during the AOC listed in Table 1.

TABLE 1 The impact of dynamic setting and dynamic clustering on DN during different operation scenarios.

No.	SS-IBRs dynamic setting	IBRs in a dynamic cluster	Max_{DY-LO} and violation limit	Settings time-duration	SS config	All IBRs used energy (%)	Violation
1	All-IBRs	Static cluster	IEEE Std. (1.05–1.1 pu)	11:00–14:30	SS 4321	731.45	No
2	All-IBRs	Static cluster	Default (1.095–1.1 pu)	11:00–14:30		1129.15	All S/S
3	SS 1	NB	(1.090–1.090 pu)	11:00–11:25		1030.57	No
	SS 2, 3 & 4	AS, DT & UC	(1.080–1.085 pu)	11:00–11:50			
4	All-IBRs	Static cluster	IEEE Std. (1.05–1.1 pu)	11:00–14:30	SS 1234	924.18	No
5	All-IBRs	Static cluster	Default (1.095–1.10 pu)	11:00–14:30		1328.38	No

TABLE 2 Percentage of energy used by the IBR during different scenarios.

		Sun-energy utilized (%)				
		SS 4321 configuration			**SS 1234 configuration**	
SS No.	**Customer (IBR)**	**IEEE**	**Default**	**No (3)**	**IEEE**	**Default**
SS (1)	OB1 (IBR-R)	47.76	85.08	94.11	66.46	99.88
	OB2 (IBR-M)	42.99	74.83	84.02	60.87	99.41
	OB3 (IBR-N)	50.48	88.12	73.45	69.07	99.88
	OB4 (IBR-B)	54.11	90.99	74.92	71.48	99.83
SS (2)	BLD1 (IBR-S)	57.64	78.23	68.88	67.16	90.37
	BLD10 (IBR-O)	55.66	69.53	72.29	63.97	79.27
	BLD2 (IBR-A)	48.35	92.12	63.43	65.45	99.84
	BLD3 (IBR-Z)	37.09	44.56	51.10	53.16	86.78
	BLD4 (IBR-V)	40.72	52.35	56.01	54.55	80.24
SS (3)	BLD5 (IBR-T)	70.25	99.87	76.47	75.82	99.88
	BLD8 (IBR-D)	78.60	99.86	99.86	82.93	99.87
	PB8 (IBR-W)	43.74	78.06	84.76	51.86	93.48
SS (4)	OB5 (IBR-U)	53.88	97.64	68.51	72.78	99.88
	OB8 (IBR-C)	50.17	77.91	62.76	68.63	99.80
Substation violation		**NO**	**YES**	**NO**	**NO**	**NO**
Quantifying of fairness						
Sum of all (%)		**731.45**	**1129.15**	**1030.5**	**924.18**	**1328.39**
Utilization percentage (%)		**52.25**	**80.65**	**73.6**	**66.01**	**94.89**

sequently, IBRs (N B) are excluded from the cluster (return to default setting) and the other six IBRs (A S D T U C) are preserved in the cluster from 11:25 to 11:50. As substation voltage returns to normal, the six IBRs are excluded from the cluster and return to default settings. The dynamic clusters are shown in Figure 13, and their updated IBRs' settings are as indicated in Table 1. The total sum of the percentages of used available energy by all IBRs is calculated as 1030.56% (141% of the IEEE standard settings). Details of the percentage of energy used by each IBR are provided in Table 2. The last two rows in the table quantify the fairness of the proposed approach. For the S4321 configuration, the proposed approach achieved 73.6% utilization of available solar power, compared to 52% for the IEEE std. setting. This extra power has been achieved by selectively curtailing only the responsible IBRs, which are identified through clustering. The shaded cells in the table indicate clustered IBRs, those most responsible for voltage violations. These clustered IBRs experienced more curtailment compared to the "Default" case, while the remaining "non-responsible" IBRs were allowed to utilize more power fairly while avoiding voltage violation.

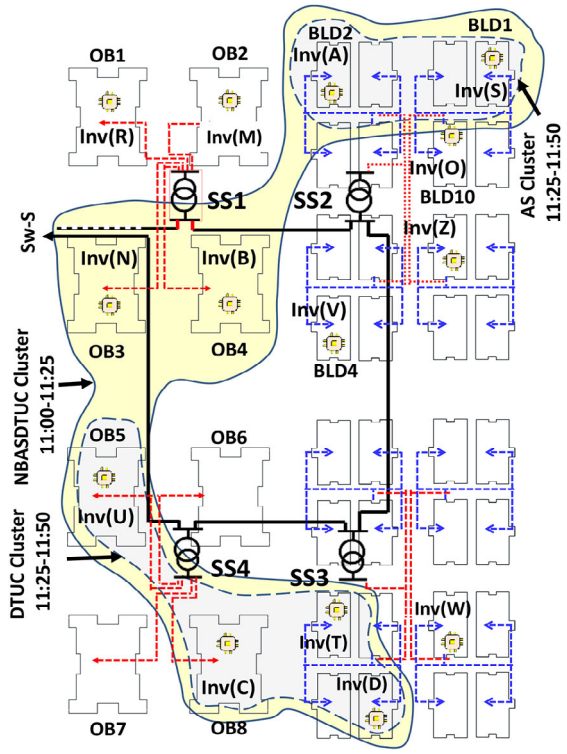

FIGURE 13 Dynamic clusters based on IBRs' sensitivity.

8.2 | The impact of the proposed technique on the DN customers without IBRs during AOC

The impact of the default setting allows all IBR owners to benefit from utilizing the maximum available sun-power. The reflection of this benefit on other adjacent customers without IBRs is also investigated. Customers connected to SS3 and do not have IBRs are considered in this investigation. Two customers (PB 6 and 7) are connected directly with 0.4 kV feeders to SS3. During AOC, the voltages on the substation (E_{SS3}), and the pillar boxes (E_{PB6} and E_{PB7}) are monitored during the two operation settings (scenario 2 and scenario 3). As the proposed method controls the voltage rise at both the substation level and IBR-owners level, other adjacent customers in the DN will have a controlled voltage within the allowed standard limit as well. While during scenario 2 (default setting case) a voltage rise on E_{SS3}, E_{PB6} and E_{PB7} was observed; enabling dynamic clustering (scenario 3) maintains voltages for all customers (with/without IBRs) to be within the standard limit. The impact of dynamic setting (scenario 2) and dynamic clustering (scenario 3) on E_{SS3}, E_{PB6} and E_{PB7} during the time-duration 11:00 to 14:30 is illustrated in Figure 14. The figure shows that the proposed method maintains voltages of adjacent customers without IBRs below 1.10 pu at all times during scenario 3.

8.3 | The impact of the proposed technique on the distribution system during NOC

As the substations reconfigure to SS 1234 (with SS1 becoming upstream and SS4 downstream), the power flow in the 11 kV feeder changes direction and magnitude while the substation bus voltage changes magnitude. Due to the long 11 kV feeder from the switching station to the SS1, no violation is detected at any substation. During this configuration, the same loads, sun-power, and 0.4 kV feeders of the previous configuration are used. Two settings' scenarios as listed in Table 1 are implemented: scenario 4 using IEEE std. fixed setting and scenario 5 of the default setting.

Applying the default setting results in a sensitivity contribution (SC_j) of similar trends as compared to those generated during scenario 3 (with substation configuration SS 4321 in Figure 8b). However, the magnitudes of SC_j during SS 1234 configuration show lower values due to the long SWS-SS1 feeder and resulted reductions in voltage values at the substation buses. On the other hand, the IBRs benefit fairly from the available sun-power with a utilization percentage of the available energy by all IBRs of 94.89% (scenario 5) as compared to 66.01% for IEEE std. setting (scenario 4). The enhancement in utilizing the sun-power using the default setting of the proposed method is quantified by a 144% increase as compared with the IEEE std. setting.

8.4 | Discussions of the results

The proposed method fairly utilized the maximum available sun-power without violating the voltage limit. This is justified mathematically in Section 2 and during the application in Section 7 while monitoring the voltage at different locations of distribution substations buses, IBRs owners' buses and non-IBRs owners as well as during different feeder configurations.

Mathematically and as presented in Section 2.1, the possible maximum dynamic low and high values are defined by the system operator based on the allowable historical range of the terminal local voltage and a predefined violation limit (marked in red dotted line) in Figure 1a. The maximum value of $E_{i,LO}$ is set to be heading the actual voltage but cannot exceed the Max_{DY-LO}, this will allow utilizing the maximum available sun-power without violating the voltage limit. However abnormal conditions might cause the actual voltage to exceed the violation limit set value. In such a case, the proposed method will force the set value $E_{i,LO}$ to smoothly move towards Max_{DY-LO} as presented in (4) to quickly limit the IBR injected power to a minimum value.

In the application section, the simulated system is tested considering changed loads that lead to high distribution substation voltages. The proposed dynamic cluster and dynamic setting method shows excellent results as illustrated in Figures 11 and 12. The method is fairly utilized the maximum available sun-power without violating the voltage limit. The method satisfies the requirement defined in the IEEE std. 1547 where voltages between 0.88 and 1.10 pu was guaranteed in order to allow the IBR continuous operation as clearly illustrated for all IBRs in Figure 11. Furthermore, at the distribution substations buses, the proposed dynamic cluster and dynamic setting method as compared with IEEE std. method shows a flexible control to regulate the bus voltages based on time-duration of voltage

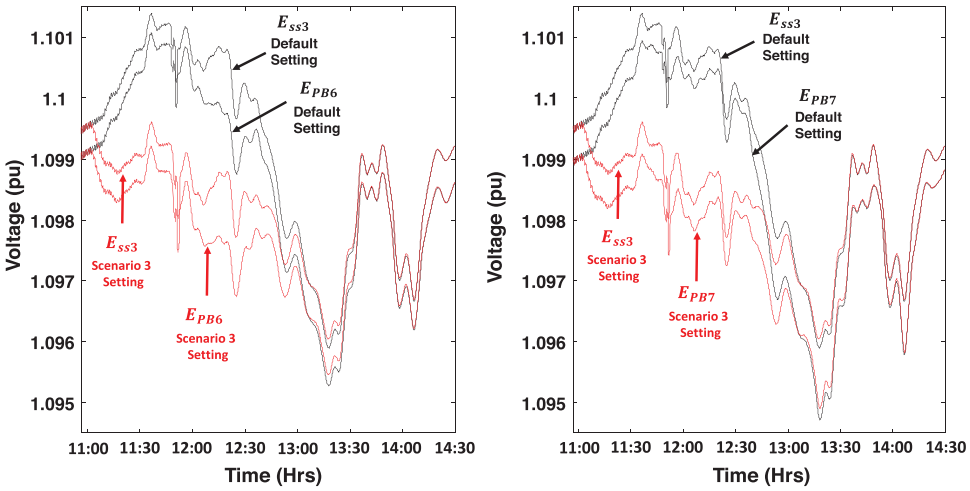

FIGURE 14 The impact of the default setting and Dynamic cluster setting on non-IBR owner customers.

rise, the IBRs included in the dynamic cluster and set value of the Max_{DY-LO} and violation limit. The method shows 141% increase of fair utilization of sun-power energy as well as IBRs continuous operation voltage. Moreover, fairness and voltage control with non-IBRs owner is also considered. The impact of the default setting and dynamic cluster setting on non-IBR owner customers is illustrated in Figure 14. The results show that being fair with IBR owner to utilize the maximum available sun-power will not impact voltage limit of other end-users, non-IBR owners, connected in the same network.

The proposed approach guarantees voltage control of all end-users and distribution substation buses such that the voltage rise is limited constrained that this rise has resulted from the IBRs injected power. However, if the voltage rise is due to a primary system high voltage level, then controlling IBRs injected power to minimum values might not provide a solution.

9 | CONCLUSION

The voltage regulation approach offered in this paper proposes flexible local or remote management of the IBRs that satisfy fair financial benefits among customers without violating the voltage standard limits. The proposed algorithm overcomes the fairness constraint in terms of IBR location, assigned power limit, and inverter terminal voltage. The local and remote management are aligned in the proposed approach to offer dynamic settings of IBRs considering the mutual sensitivity among them as well as the status of the whole network voltage condition. The IBRs' droop control and their mutual sensitivity measures are used to define the dynamic clusters' boundaries of the most sensitive IBRs. The dynamic settings of a limited number of IBRs within the dynamic cluster result in a significant contribution to overcoming voltage rise problems without impacting fairness. The stand-alone LoRaWAN communication is implemented to facilitate the involvement of a 3-party (aggregator) in such business of the energy market. This communication tool is investigated within the DN steady-state operation during voltage-rise time-frame and successfully enables a data-driven, monitoring, processing, and remotely broadcast of dynamic settings to IBRs within the dynamic cluster.

AUTHOR CONTRIBUTIONS

All authors have contributed equally to ideas formulation, development of the methodology, and original draft writing.

ACKNOWLEDGEMENTS

Open access publishing facilitated by Deakin University, as part of the Wiley - Deakin University agreement via the Council of Australian University Librarians.

CONFLICT OF INTEREST STATEMENT

The authors declare no conflict of interest.

DATA AVAILABILITY STATEMENT

Data sharing is not applicable to this article as no new data were created or analyzed in this study.

ORCID

Ameen Gargoom https://orcid.org/0000-0002-4635-4993

REFERENCES

1. Qammar, N., Arshad, A., Miller, R.J., Mahmoud, K., Lehtonen, M.: Machine learning based hosting capacity determination methodology for low voltage distribution networks. IET Gen. Trans. Distrib. 18, 911–920 (2024). https://doi.org/10.1049/gtd2.12933
2. Sharma, V., Haque, M.H., Aziz, S.M., Kauschke, T.: Smart inverter and battery storage controls to reduce financial loss due to overvoltage-induced PV curtailment in distribution feeders. Sustain. Energy Grids Netw. 34, 101030 (2023)
3. Zhang, Z., Dou, C., Yue, D., Zhang, B., Zhao, P.: High-economic PV power compensation algorithm to mitigate voltage rise with minimal curtailment. Int. J. Electr. Power Energy Syst. 125, 106401 (2021). https://doi.org/10.1016/j.ijepes.2020.106401
4. Olivier, F., Aristidou, P., Ernst, D., Van Cutsem, T.: Active management of low-voltage networks for mitigating overvoltages due to photovoltaic

units. IEEE Trans. Smart Grid 7(2), 926–936 (2016). https://doi.org/10.1109/TSG.2015.2410171
5. Kharrazi, A., Sreeram, V., Mishra, Y.: Assessment techniques of the impact of grid-tied rooftop photovoltaic generation on the power quality of low voltage distribution network—a review. Renewable Sustainable Energy Rev. 120, 109643 (2020). https://doi.org/10.1016/j.rser.2019.109643
6. Australian Energy Regulator: Distribution Determination 2021 to 2026, Attachment 9 Capital expenditure sharing scheme (2021)
7. Lal, N.N., Brown, L.: Give a little to get a little: A DER Bill of Rights and Responsibilities provides the social license for participation and control in DER-dominated grids—an Australian example. The Electricity Journal 36(4), 107265 (2023)
8. Stringer, N., Haghdadi, N., Bruce, A., MacGill, I.: Fair consumer outcomes in the balance: Data driven analysis of distributed PV curtailment. Renewable Energy 173, 972–986 (2021)
9. IEEE Standard for Interconnection and Interoperability of Distributed Energy Resources with Associated Electric Power Systems Interfaces, IEEE Std 1547–2018 (Revision of IEEE Std 1547–2003), pp. 1–138 (2018). https://doi.org/10.1109/IEEESTD.2018.8332112
10. Procopiou, A.T., Ochoa, L.F.: On the limitations of volt-var control in PV-rich residential LV networks: A UK case study. In: 2019 IEEE Milan PowerTech, Milan, Italy, pp. 1–6. IEEE, Piscataway (2019). https://doi.org/10.1109/PTC.2019.8810797
11. Vadavathi, A.R., Hoogsteen, G., Hurink, J.: PV inverter-based fair power quality control. IEEE Trans. Smart Grid 14(5), 3776–3790 (2023). https://doi.org/10.1109/TSG.2023.3244601
12. Xu, S., Xue, Y., Chang, L.: Review of power system support functions for inverter-based distributed energy resources-standards, control algorithms, and trends. IEEE Open J. Power Electron. 2, 88–105 (2021)
13. Zhan, S., Morren, J., Akker, W.V.D., Molen, A.V.D., Paterakis, N.G., Slootweg, J.G.: Fairness-Incorporated Online Feedback Optimization for Real-Time Distribution Grid Management. IEEE Trans. Smart Grid 15(2), 1792–1806 (2024)
14. Tonkoski, R., Lopes, L.A.C., El-Fouly, T.H.M.: Coordinated active power curtailment of grid connected PV inverters for overvoltage prevention. IEEE Trans. Sustainable Energy 2(2), 139–147 (2011). https://doi.org/10.1109/TSTE.2010.2098483
15. Latif, A., Gawlik, W., Palensky, P.: Quantification and mitigation of unfairness in active power curtailment of rooftop photovoltaic systems using sensitivity based coordinated control. Energies 9, 436 (2016). https://doi.org/10.3390/en9060436
16. Ghasemi, M.A., Parniani, M.: Prevention of distribution network overvoltage by adaptive droop-based active and reactive power control of PV systems. Electr. Power Syst. Res. 133, 313–327 (2016). https://doi.org/10.1016/j.epsr.2015.12.030
17. Alyami, S., Wang, Y., Wang, C., Zhao, J., Zhao, B.: Adaptive real power capping method for fair overvoltage regulation of distribution networks with high penetration of PV systems. IEEE Trans. Smart Grid 5(6), 2729–2738 (2014)
18. Mousavi, M., Wu, M.: A DSO framework for market participation of DER aggregators in unbalanced distribution networks. IEEE Trans. Power Syst. 37(3), 2247–2258 (2022)
19. Lusis, P., Andrew, L.L.H., Chakraborty, S., Liebman, A., Tack, G.: Reducing the unfairness of coordinated inverter dispatch in PV-rich distribution networks. In: Proceedings of IEEE Milan PowerTech, pp. 1–6. IEEE, Piscataway (2019)
20. Liu, M.Z., et al.: On the fairness of PV curtailment schemes in residential distribution networks. IEEE Trans. Smart Grid 11(5), 4502–4512 (2020)
21. Gebbran, D., Mhanna, S., Ma, Y., Chapman, A.C., Verbič, G.: Fair coordination of distributed energy resources with volt-var control and pv curtailment. Appl. Energy 286, 116546 (2021)
22. Poudel, S., Mukherjee, M., Reiman, A.P.: A fairness-based distributed energy coordination for voltage regulation in distribution systems. In: 2022 IEEE Green Technologies Conference (GreenTech), pp. 45–50. IEEE, Piscataway (2022)
23. Mai, T.T., Haque, A.M.M., Vergara, P.P., Nguyen, P.H., Pemen, G.: Adaptive coordination of sequential droop control for PV inverters to mitigate voltage rise in PV-Rich LV distribution networks. Electr. Power Syst. Res. 192, 106931 (2021). https://doi.org/10.1016/j.epsr.2020.106931
24. Vadavathi, A.R., Hoogsteen, G., Hurink, J.L.: Comparison of fairness based coordinated grid voltage control methods for PV inverters. In: 2021 IEEE PES Innovative Smart Grid Technologies Europe (ISGT Europe), pp. 1–5. IEEE, Piscataway (2021). https://doi.org/10.1109/ISGTEurope52324.2021.9639982
25. Sadnan, R., Poudel, S., Mukherjee, M., Slay, T.E., Reiman, A.P.: Bisection method for fairness-aware distributed PV curtailment in power distribution systems. In: 2023 IEEE Power & Energy Society General Meeting (PESGM), pp. 1–5. IEEE, Piscataway (2023). https://doi.org/10.1109/PESGM52003.2023.10252260
26. Poudel, S., Mukherjee, M., Sadnan, R., Reiman, A.P.: Fairness-aware distributed energy coordination for voltage regulation in power distribution systems. IEEE Trans. Sustainable Energy 14(3), 1866–1880 (2023). https://doi.org/10.1109/TSTE.2023.3252944
27. Osorio, A., Calle, M., Soto, J.D., Candelo-Becerra, J.E.: Routing in LoRaWAN: Overview and challenges. IEEE Commun. Mag. 58(6), 72–76 (2020). https://doi.org/10.1109/MCOM.001.2000053
28. Premsankar, G., Ghaddar, B., Slabicki, M., Francesco, M.D.: Optimal configuration of lora networks in smart cities. IEEE Trans. Ind. Inf. 16(12), 7243–7254 (2020). https://doi.org/10.1109/TII.2020.2967123
29. Lee, H.-C., Ke, K.-H.: Monitoring of large-area iot sensors using a LoRa wireless mesh network system: Design and evaluation. IEEE Trans. Instrum. Meas. 67(9), 2177–2187 (2018). https://doi.org/10.1109/TIM.2018.2814082
30. Gargoom, A., Elmusrati, M., Gaouda, A.: Enhancing the operation of smart inverters with pmu and data concentrators. Int. J. Electr. Power Energy Syst. 140, 108077 (2022). https://doi.org/10.1016/j.ijepes.2022.108077
31. LoRaWAN Specification (v1.0.3) (March 2022). https://lora-alliance.org/resourcehub/lorawan-specification-v1-0-3/. Accessed: 3 Nov 2022
32. Varsier, N., Schwoerer, J.: Capacity limits of LoRaWAN technology for smart metering applications. In: 2017 IEEE International Conference on Communications (ICC), pp. 1–6. IEEE, Piscataway (2017). https://doi.org/10.1109/ICC.2017.7996383
33. Laveyne, J.I., Zwaenepoel, B., Van Eetvelde, G., Vandevelde, L.: Potential of domestically provided ancillary services to the electrical grid. In: 2017 52nd International Universities Power Engineering Conference (UPEC), pp. 1–6. IEEE, Piscataway (2017). https://doi.org/10.1109/UPEC.2017.8231906
34. Nakutis, Z.˘., Kuzas, P., Rybelis, T., Grimaila, V., Daunoras, V.: A technique of synchronization of distributed energy measurement in low voltage electrical grid. In: 2018 IEEE 9th International Workshop on Applied Measurements for Power Systems (AMPS), pp. 1–6. IEEE, Piscataway (2018). https://doi.org/10.1109/AMPS.2018.8494885
35. Sheeba, R. et al.: Real-time monitoring of energy meters using cloud storage. 2021 IEEE International Power and Renewable Energy Conference (IPRECON), pp. 1–5. Kollam, India (2021). https://doi.org/10.1109/IPRECON52453.2021.9640636
36. Jose, J.: Real-time monitoring of energy meters using cloud storage. In: 2021 IEEE International Power and Renewable Energy Conference (IPRECON), pp. 1–5. IEEE, Piscataway (2021). https://doi.org/10.1109/IPRECON52453.2021.9640636
37. Sisinni, E., Bellagente, P., Depari, A., Ferrari, P., Flammini, A., Marella, S., Pasetti, M., Rinaldi, S., Cagiano, A.: A new LoRaWAN adaptive strategy for smart metering applications. In: 2020 IEEE International Workshop on Metrology for Industry 4.0 & IoT, pp. 690–695. IEEE, Piscataway (2020). https://doi.org/10.1109/MetroInd4.0IoT48571.2020.9138226
38. Lin, T., Baohao, C., Weiming, G., Guoyi, Z., Long, W.: Deployment and performance verification of 5 g smart grid based on lora. In: 2021 4th International Conference on Information Communication and Signal Processing (ICICSP), pp. 538–542. IEEE, Piscataway (2021). https://doi.org/10.1109/ICICSP54369.2021.9611908
39. Rizzi, M., Ferrari, P., Flammini, A., Sisinni, E.: Evaluation of the IoT LoRaWAN solution for distributed measurement applications. IEEE Trans. Instrum. Meas. 66(12), 3340–3349 (2017). https://doi.org/10.1109/TIM.2017.2746378

40. Kuzlu, M., Pipattanasomporn, M., Rahman, S.: Communication network requirements for major smart grid applications in han, nan and wan. Comp. Netw. 67, 74–88 (2014). https://doi.org/10.1016/j.comnet.2014.03.029
41. OMNeT++ simulation models. https://omnetpp.org/download/models-and-tools. Accessed 12 Nov 2022
42. INET framework. https://inet.omnetpp.org/. Accessed 12 Nov 2022
43. Yan, R., Xing, Q., Xu, Y.: Multi-agent safe graph reinforcement learning for PV inverters-based real-time decentralized volt/var control in zoned distribution networks. IEEE Trans. Smart Grid 15(1), 299–311 (2024). https://doi.org/10.1109/TSG.2023.3277087
44. Zhang, R., Haoming, L., Meng, Y., Jian, W., Jie, S.: Network partitioning and hierarchical voltage regulation for distribution networks using holomorphic embedding method-based sensitivity. IET Gen. Trans. Distrib. 17(3), 604–620 (2023)
45. Wang, Z., Tan, W., Li, H., Ge, J., Wang, W.: A voltage coordination control strategy based on the reactive power-active network loss partitioned aggregation domain. Int. J. Electr. Power Energy Syst. 144, 108585 (2023)

How to cite this article: Gargoom, A., Elmusrati, M., Gaouda, A.: Dynamic sensitivity-based clustering of distributed energy resources using LoRaWAN technology for voltage regulation in distribution networks. IET Gener. Transm. Distrib. 1–20 (2024). https://doi.org/10.1049/gtd2.13343